Computational Materials Science 99 (2015) 396–416

Contents lists available at ScienceDirect

Computational Materials Science

journal homepage: www.elsevier.com/locate/commatsci

A numerical study on chloride migration in cracked concrete using multi-component ionic transport models

Qing-feng Liu [a,b,*], Jian Yang [a,b,e], Jin Xia [c], Dave Easterbrook [d], Long-yuan Li [d], Xian-Yang Lu [a,b]

[a] State Key laboratory of Ocean Engineering, Shanghai Jiao Tong University, Shanghai 200240, PR China
[b] School of Naval Architecture, Ocean & Civil Engineering, Shanghai Jiao Tong University, Shanghai 200240, PR China
[c] Institute of Structural Engineering, Zhejiang University, Hangzhou, PR China
[d] School of Marine Science and Engineering, University of Plymouth, PL4 8AA, UK
[e] School of Civil Engineering, University of Birmingham, B15 2TT, UK

ARTICLE INFO

Article history:
Received 4 September 2014
Received in revised form 27 December 2014
Accepted 9 January 2015
Available online 31 January 2015

Keywords:
Numerical modelling
Concrete
Crack
Chloride
Migration
Heterogeneous
Multi-phase
Multi-species
Ionic interaction
Binding

ABSTRACT

This paper presents a numerical study on the mechanism of chloride migration in cracked concrete. Unlike most of existing work, this study utilises multi-component ionic transport models to reflect the influence of ionic interactions by coupling the mass conservation and Poisson's equations. To provide a better understanding of the influences caused by multi-component migration and concrete cracking, two categories of geometry samples are displayed and discussed respectively. Finally, through a comparatively overall numerical exploration, which includes external voltage, ionic interactions, heterogeneous nature, binding effect and multiple cracks arrangement, a series of important transport features, which cannot be revealed previously from existing cracked concrete models, are highlighted.

1. Introduction

Nowadays, durability problem has received more and more attention in the concrete industry. It is well known that the performance of reinforced concrete (RC) structures will be significantly influenced by the penetration of ions, especially chloride ions. This deterioration caused by chloride-induced corrosion of reinforcing steel is even serious when the concrete has cracks. Cracking is an inevitable phenomenon for RC structures and can be generated due to various reasons, i.e., plastic and restrained shrinkage, thermal and mechanical loading, expansive degradation reactions, improper design, etc.

To assess the effect of cracking characteristics on chloride diffusion in concrete, a number of studies [1–12] have been reported, in which traditional approaches including analytical and/or experimental methods were used. However, note that concrete is a heterogeneous material with complicated microstructure organisation. For analytical studies, the main shortcoming is that they could only focus on the transport of ions in a 1-D single-phase medium (i.e., the cement or mortar matrix), neglecting the impact of other meso- or micro-structures in concrete. Moreover, due to the high nonlinear level of the problem of multi-component ionic transport, almost all existing analytical models consider the transport of only a single-species, i.e. the chloride ions. For experimental studies, though they can provide wider and valuable data, it is still very difficult for them to reveal individual effects of different factors because of the interactions between different factors. Also, most of testing methods are expensive and time-consuming, especially for the high-performance concrete specimens.

Hence, with respect to the abovementioned issues, as well as the fast advance of computer science and progress of computational mathematics, today's researchers tend to adopt the numerical technique to gain a better understanding of the mechanism of chloride transport in cracked concrete [13–18]. For example, Leung and Hou [13] developed a 2-D single-phase concrete model with cracks for investigating the chloride-induced reinforcement corrosion. Marsavina et al. [14] examined the influence of artificial

* Corresponding author at: School of Naval Architecture, Ocean & Civil Engineering, Shanghai Jiao Tong University, Shanghai 200240, PR China. Tel.: +86 1394 2035 131.
E-mail addresses: henrylqf@163.com, liuqf@sjtu.edu.cn (Q.-f. Liu).

http://dx.doi.org/10.1016/j.commatsci.2015.01.013
0927-0256/

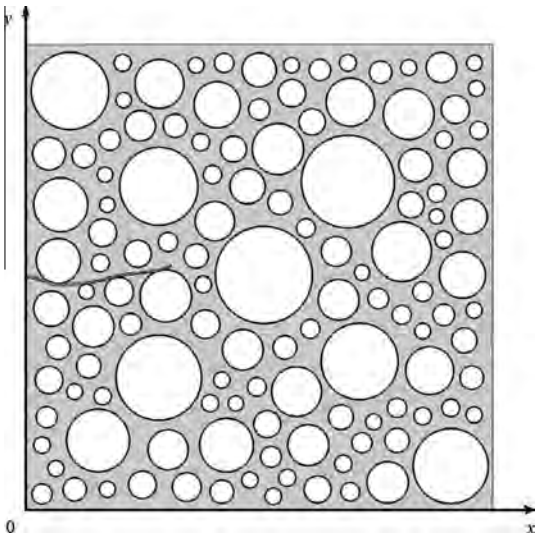

Fig. 1. Geometry of 3-phase heterogeneous concrete model with mesocrack.

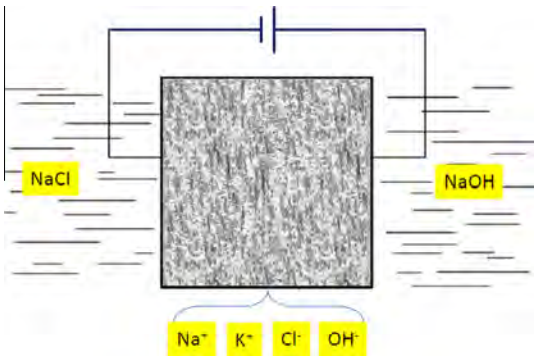

Fig. 3. Schematic representation of 2-D plain concrete specimen in a RCM test.

Table 2
Initial and boundary conditions of individual species.

Field variables		Potassium	Sodium	Chloride	Hydroxide	Electrostatic potential
Concentration boundary conditions, mol/m^3	$x = 0$	0	520	520	0	0
	$x = L$	0	300	0	300	24 V
Flux boundary conditions	$y = 0$	$J = 0$	$J = 0$	$J = 0$	$J = 0$	$\partial\Phi/\partial y = 0$
	$y = L$	$J = 0$	$J = 0$	$J = 0$	$J = 0$	$\partial\Phi/\partial y = 0$
Initial conditions, mol/m^3	$t = 0$	200	100	0	300	0

cracks on the chloride penetration in concrete using a 3-D finite element analysis model. However, the model developed was based on a single phase for which the concrete was treated as a homogenous material. Wang and Ueda [15] proposed a 2-D mesoscale transport model for investigating chloride diffusion in cracked concrete, in which the concrete was treated as a three-phase composite, consisting of aggregate, mortar, and interfacial transition zone (ITZ). It was found that chloride ions can penetrate into cracks with a much higher speed than they do into other phases. Šavija et al. [16] presented a further simulation with a 3-D geometry based on lattice fracture model [19–22] to emphasise that cracked concrete is highly inhomogeneous and their transport properties would show significant local variations. Mesoscale finite element models, originally developed for the stress analysis of concrete [23,24], have recently been applied to predict the transport

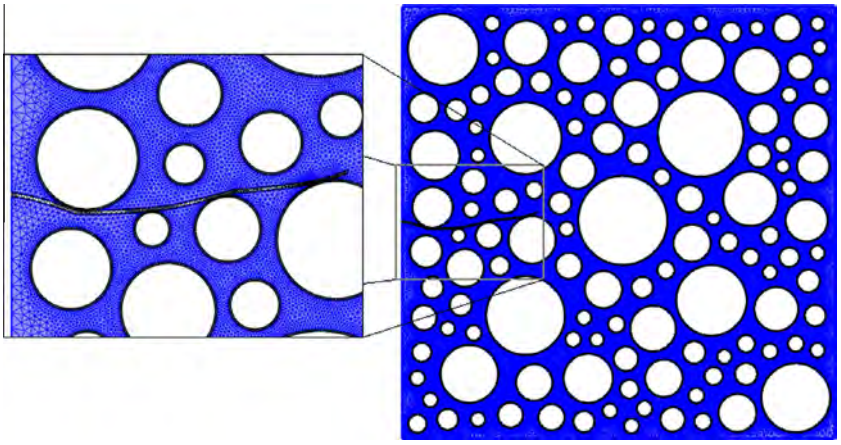

Fig. 2. Finite element mesh.

Table 1
Ionic transport properties in different phases.

Field variables	Potassium (mol/m^3)	Sodium (mol/m^3)	Chloride (mol/m^3)	Hydroxide (mol/m^3)
Charge number	1	1	−1	−1
Diffusion coefficient in aggregates, D_A	0	0	0	0
Diffusion coefficient in bulk mortar, $D_B \times 10^{-10}$ m^2/s	3.914	2.668	4.064	10.52
Diffusion coefficient in ITZs, $D_I \times 10^{-9}$ m^2/s	1.174	0.800	1.219	3.156
Diffusion coefficient in crack, $D_C \times 10^{-8}$ m^2/s	2.348	1.601	2.438	6.312
Diffusion coefficient in damage zone, $D_D \times 10^{-8}$ m^2/s	0.783	0.534	0.921	2.104

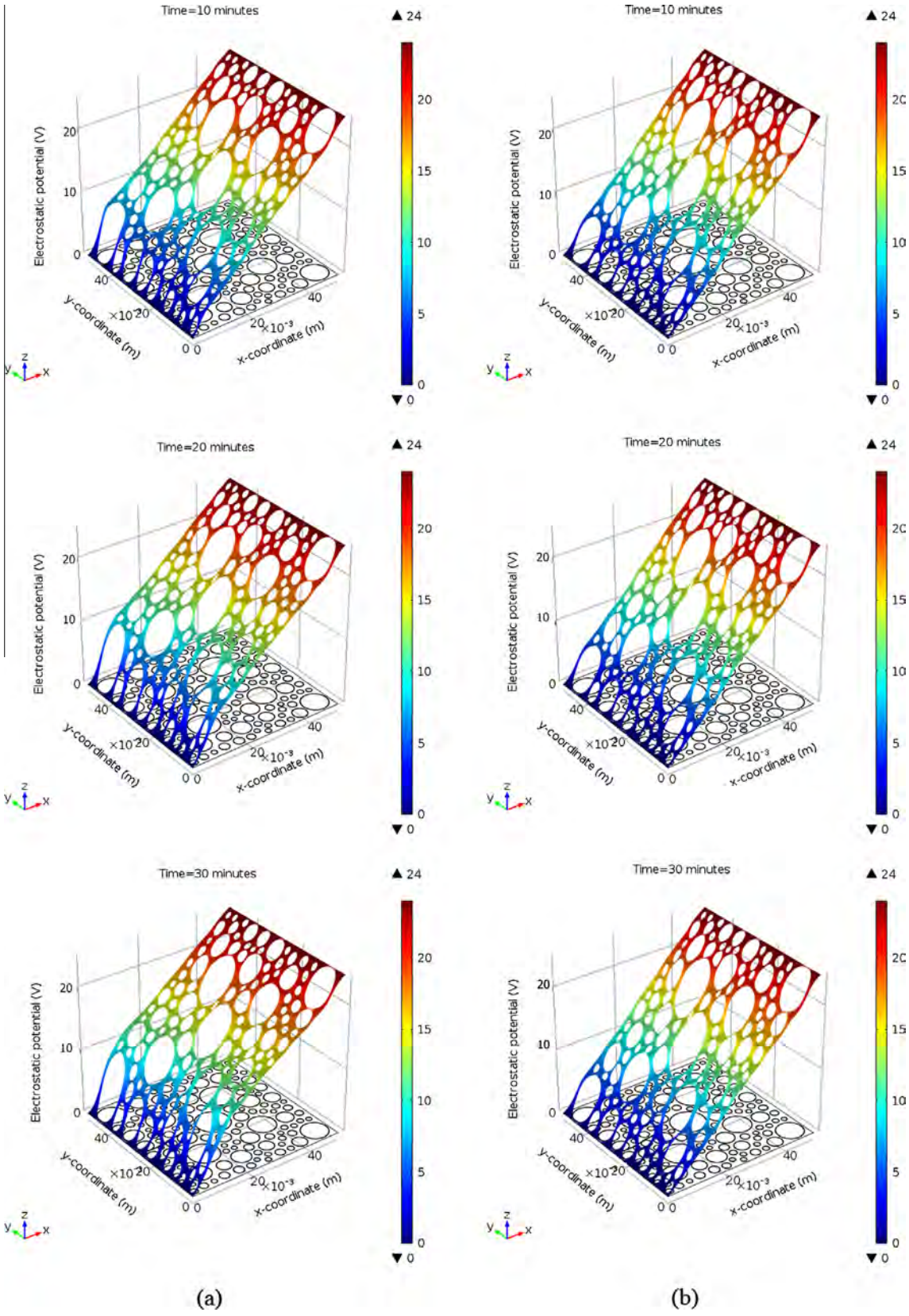

Fig. 4. Comparisons of electrostatic potential distribution between (a) multi- and (b) single-component models.

properties in concrete with and without cracks [25,26]. To quantify the effect of cracks on chloride diffusion in concrete, Bentz et al. [17] explored another 2-D single-phase model for estimating the local chloride concentration as a function of crack width and depth, from which the influence of cracks on concrete service life is predicted. Their study also showed that the chloride binding by the

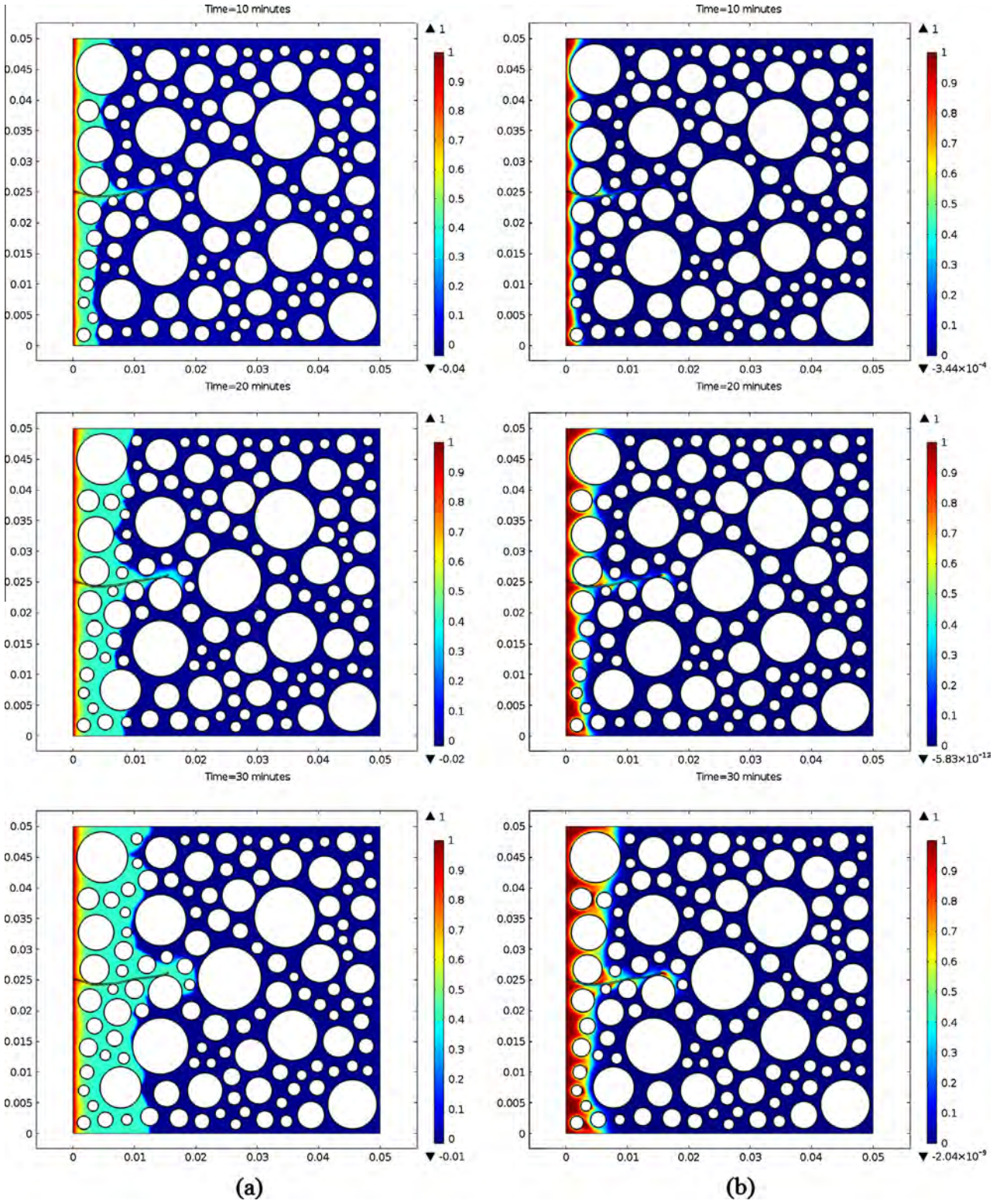

Fig. 5. Comparisons of normalized chloride concentration distributions between (a) multi- and (b) single-component models.

cement paste plays a significant role in slowing the ingress of chlorides and should be taken into account in the modelling.

Above numerical studies considered a diffusion problem and employed the Fick's second law to govern the chloride penetration in cracked concrete. In view of the long duration of diffusion tests and the need of electrochemical rehabilitation, the action of externally applied electric field is prevalently involved in a bunch of numerical models of chloride transport in concrete [27–41]. These models extended the ionic diffusion to a more complicated migration dominated process, which follows the applications of the rapid chloride migration (RCM) test [42–44] and the electrochemical chloride removal/extraction (ECR/ECE) treatment [45]. However, the convection-dominated diffusion equations caused due to the presence of external electric field can create some numerical

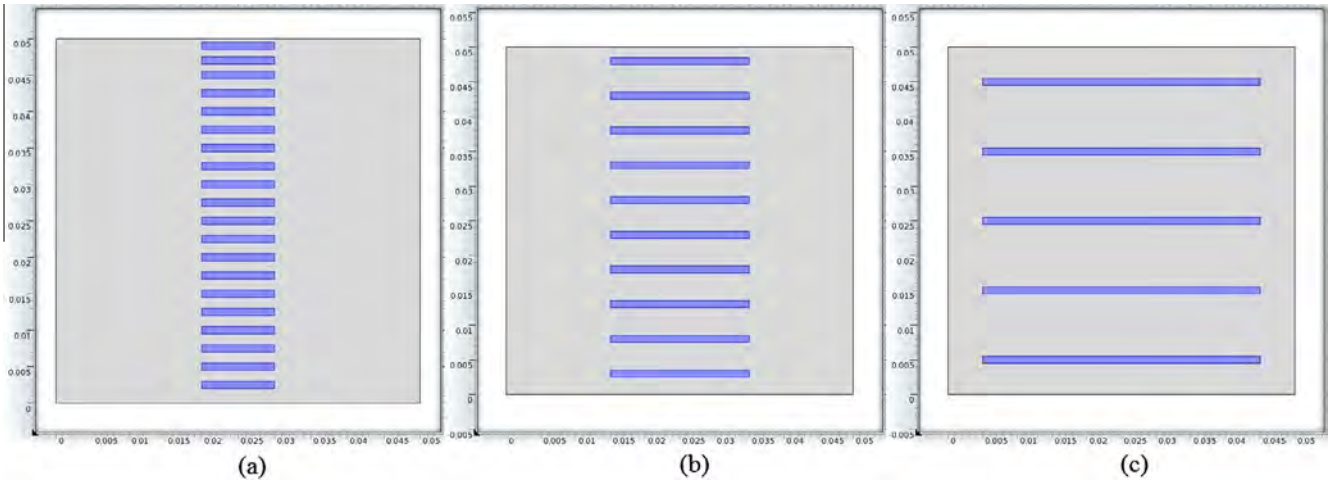

Fig. 6. Geometry of cracked concrete model with the same width (1 mm) and volume fraction (V_D = 0.08) but different depths of damage zone ((a) 10 mm, (b) 20 mm and (c) 40 mm).

difficulties both in meshing and computing due to the Peclet number issue [18,31,32], particularly when the structure studied involves different size zones, for instance, ITZs and cracks. In order to investigate the influence of cracking on chloride migration, more recently, Šavija et al. [18] further proposed another lattice model of micro-cracked concrete, in which the chloride transport is governed by Nernst–Planck equation. This model not only considered the external voltage to simulate the RCM test, but also allows the heterogeneous nature of concrete by distributing a certain volume fraction of aggregates within a thin-slab concrete geometry. A series of factors during the simulated test including the aggregate effect, loading stress, and artificial cracks were discussed through a set of obtained 2-D chloride distribution profiles.

The literature survey described above shows that most of existing numerical transport models applied for concrete with cracks [13–18] did not consider the interaction of ionic species involved in the concrete pore solution. It has been shown that the models with multi-species coupling controlled by Poisson's equation, which represents the true electrochemistry law for determining electrostatic potential in the transport medium, can provide more accurate results than those with only single ionic species or those consider multi-species in the pore solution but use the assumption of electro-neutrality condition [28–32]. In this paper, a numerical study is presented for theoretically investigating the mechanism of chloride migration in cracked concrete. Unlike most of existing work, this study utilises multi-component ionic transport models to reflect the influence of ionic interactions by coupling both mass conservation and Poisson equations. Two categories of concrete geometric models are investigated. The first one is for heterogeneous concrete with mortar matrix, coarse aggregates and ITZs. A single mesocrack was created in the concrete based on the same principle as used in the fracture modelling [19]. The crack is located in the edge of the concrete and follows a weak-link of the material in that region. The second one is for homogenous concrete, which ignores the aggregate and ITZ phases. The cracks in the concrete are artificial and are treated as "damage zones" with larger scale. The locations of the cracks are assumed in the middle of the geometry, which represents the concrete, that had cracks but its surface has been repaired and thus the cracks inside of the concrete remain. Additionally, in consideration of that all existing cracking models only focus on a single crack and any adjacent cracks are probably assumed to be sufficiently far away from each other [13–18], the interactive effect caused by multiple cracks is also added into the second category of the models. Note that all models used in the present study are two-dimensional. This is because the numerical difficulties arisen from the use of Poisson's equation and the geometric models involving different dimensional scales. Finally, through a comparatively overall numerical exploration, which includes external voltage, ionic interactions, heterogeneous nature, binding effect and multiple cracks arrangement, a series of important transport features, which cannot be revealed previously from existing cracked concrete models, are highlighted.

2. Theoretical background

Concrete pore solution is a multi-component electrolyte involving not only chloride ions but also other ions such as sodium, potassium, hydroxyl, sulphate, and calcium. For the cases of diffusion tests, the transport of ions in a saturated concrete is mainly driven by the concentration gradient of the species itself and can be described as Fick's first law, which is most utilised in the durability study of the cracked concrete [13–17]. When the electrostatic potential is involved such as in migration tests [42–44], the more significant driving force of ionic transport is the electrostatic potential gradient, in which case the flux of an ionic species can be expressed using the Nernst–Planck equation as follows,

$$\mathbf{J}_k = -D_k \nabla C_k - D_k C_k \frac{z_k F}{RT} \nabla \Phi \tag{1}$$

where $\mathbf{J}_k$ is the flux, C_k is the concentration, D_k is the diffusion coefficient (note that in the heterogeneous concrete model, D_k has to be defined separately in different phases), z_k is the charge number, $F = 9.648 \times 10^{-4}$ Cmol^{-1} is the Faraday constant, $R = 8.314$ J mol^{-1}K^{-1} is the ideal gas constant, $T = 298$ K is the absolute temperature, Φ is the electrostatic potential, and the subscript k represents the k-th ionic species. Assume that the concrete is saturated and there is no chemical reaction taking place between ionic species, the following mass conservation defined in unit volume of electrolyte solution for each individual ionic species can be obtained,

$$\frac{\partial C_k}{\partial t} = -\nabla \cdot \mathbf{J}_k \tag{2}$$

where t is the time. When applying the ionic transport equations from an electrolyte solution to a porous material, one has to consider the ionic binding at pore surface. Therefore, Eq. (2) need be modified as follows,

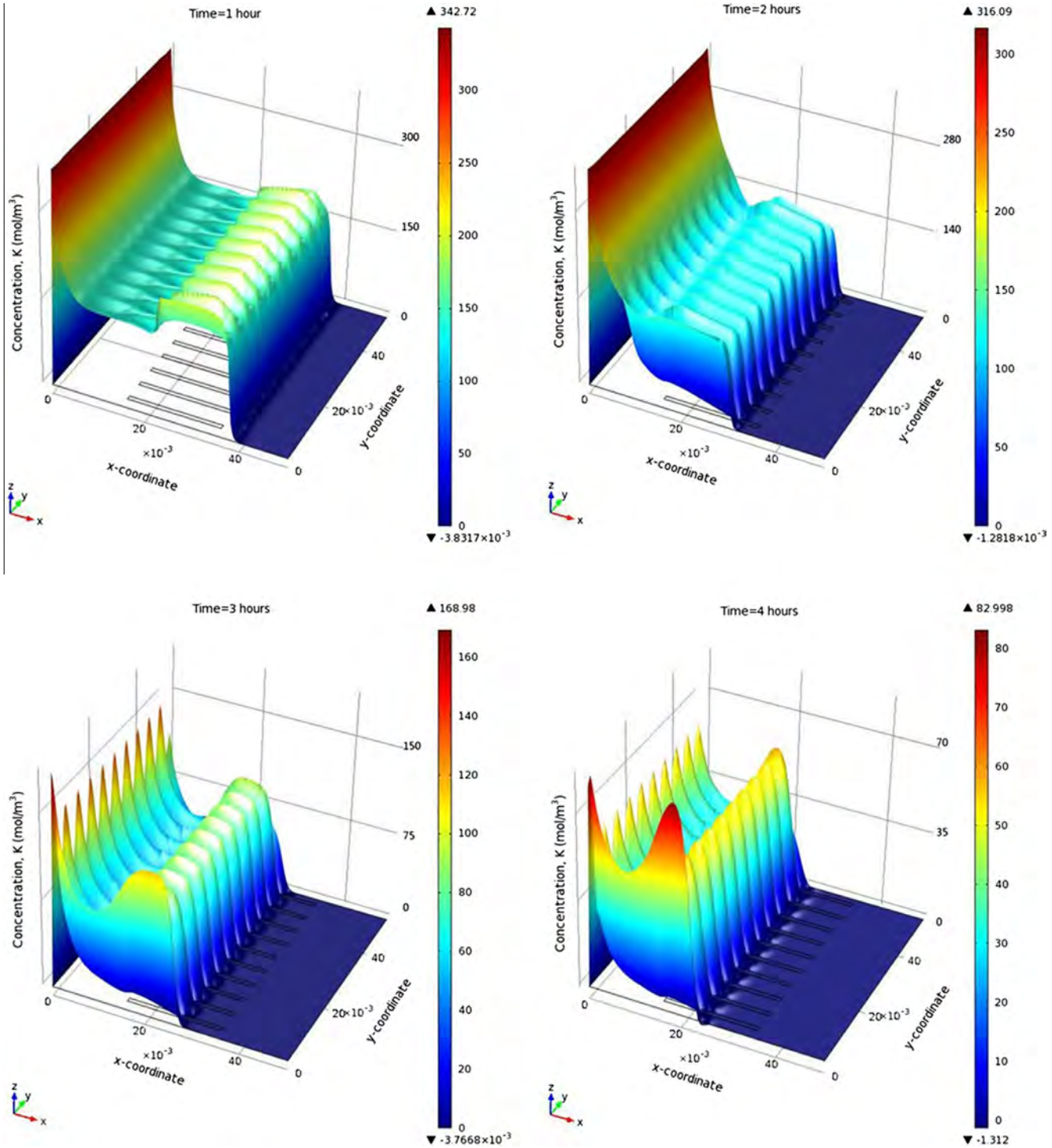

Fig. 7. Concentration distribution profiles of potassium ions.

$$\frac{\partial C_k}{\partial t} + \frac{\partial S_k}{\partial t} = -\nabla \cdot \mathbf{J}_k \tag{3}$$

where S_k is the concentration of bound ions of species k. It is suggested that the relationship between the bound and free chloride concentrations is almost independent of its transport rate and may satisfies the linear, Langmuir, or Freundlich isotherm [47] depending on its concentration. Recent work [17] highlighted the significant role of binding effect during the ingress of chlorides in cracked concrete and it is suggested to utilise a simple linear isotherm to express the relationship between free and bound ions for enhancing numerical stability,

$$S_k = \lambda C_k \tag{4}$$

where λ a is a dimensionless fitting constant. Note that for constant λ, the term $(1 + \lambda)$ can be absorbed into the time term and in this case the difference between the considerations of binding and non-binding does not affect the governing equation and is only reflected by a time factor.

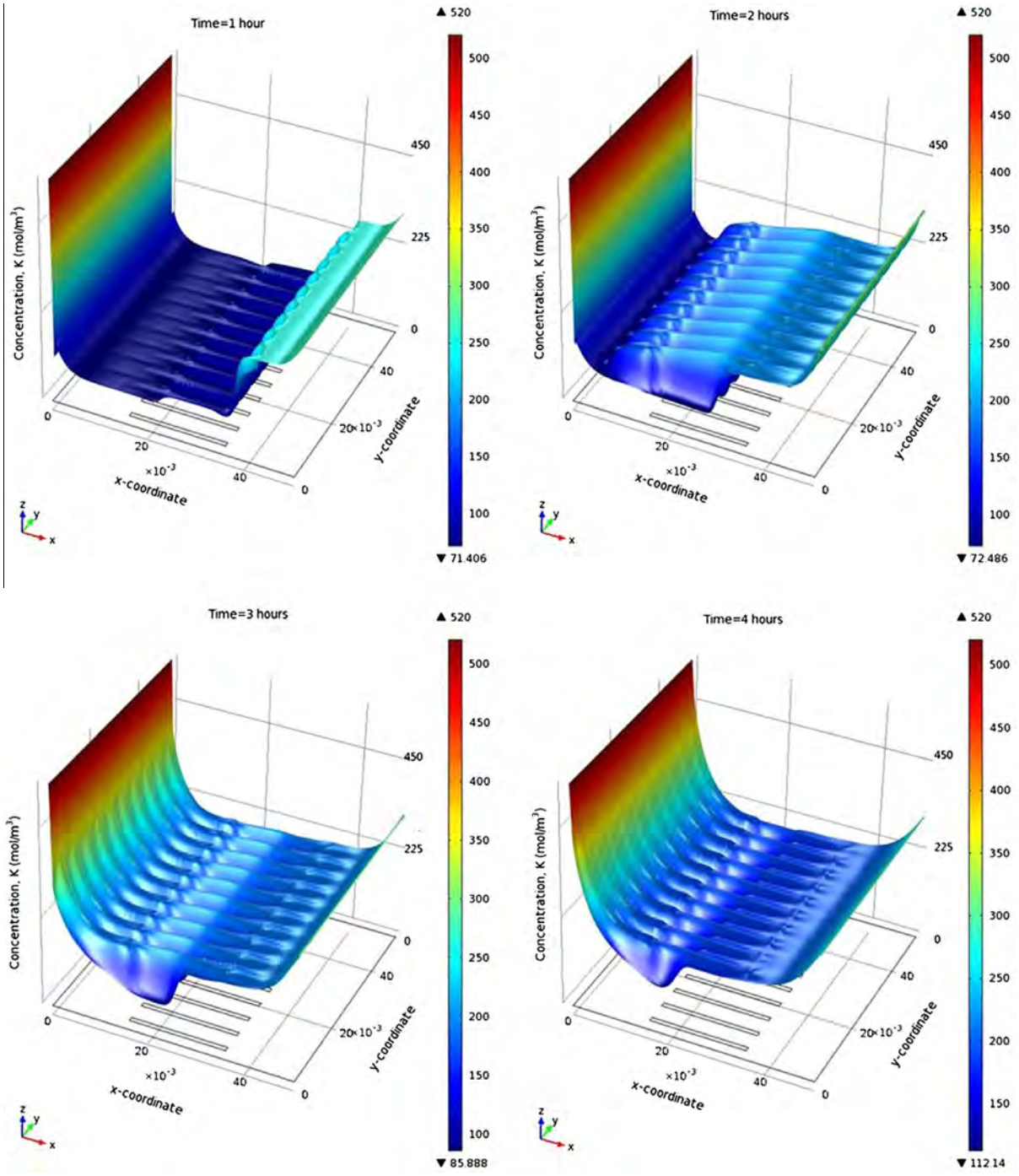

Fig. 8. Concentration distribution profiles of sodium ions.

Substituting Eqs. (1) and (4) into (3), it yields,

$$(1+\lambda)\frac{\partial C_k}{\partial t} = \nabla(D_k \nabla C_k) + \nabla\left[\left(\frac{z_k D_k F}{RT}\right) C_k \nabla \Phi\right] \tag{5}$$

In most of numerical models considering multi-species transport in concrete [27,35–41], the electrostatic potential is often determined by using the assumption of electro-neutrality condition. This implies that the spatial electrostatic potential is purely caused by the externally applied electric field and the charge balance of species occurs everywhere in the solution domain. In this case the concentration of each ionic species can be calculated independently using Eq. (5) by employing $\nabla^2 \Phi = 0$. Apparently, this assumption makes the multi-species transport behave as a single-component model, which does not reflect the actual interaction between different ionic species [46]. The essence of this issue is that, in fact, the electrostatic potential is generated by not only the externally applied electric field but also the significant internal charge imbalance between different ionic species. This charge imbalance within the concrete medium attributes to two reasons. The first one is that under the action of external electric field the cations and anions have opposite-direction movement. The second one is that the different ionic species usually have different diffusion coefficients and thus travel in different speeds in this multi-component system. In general, the generated charge imbalance

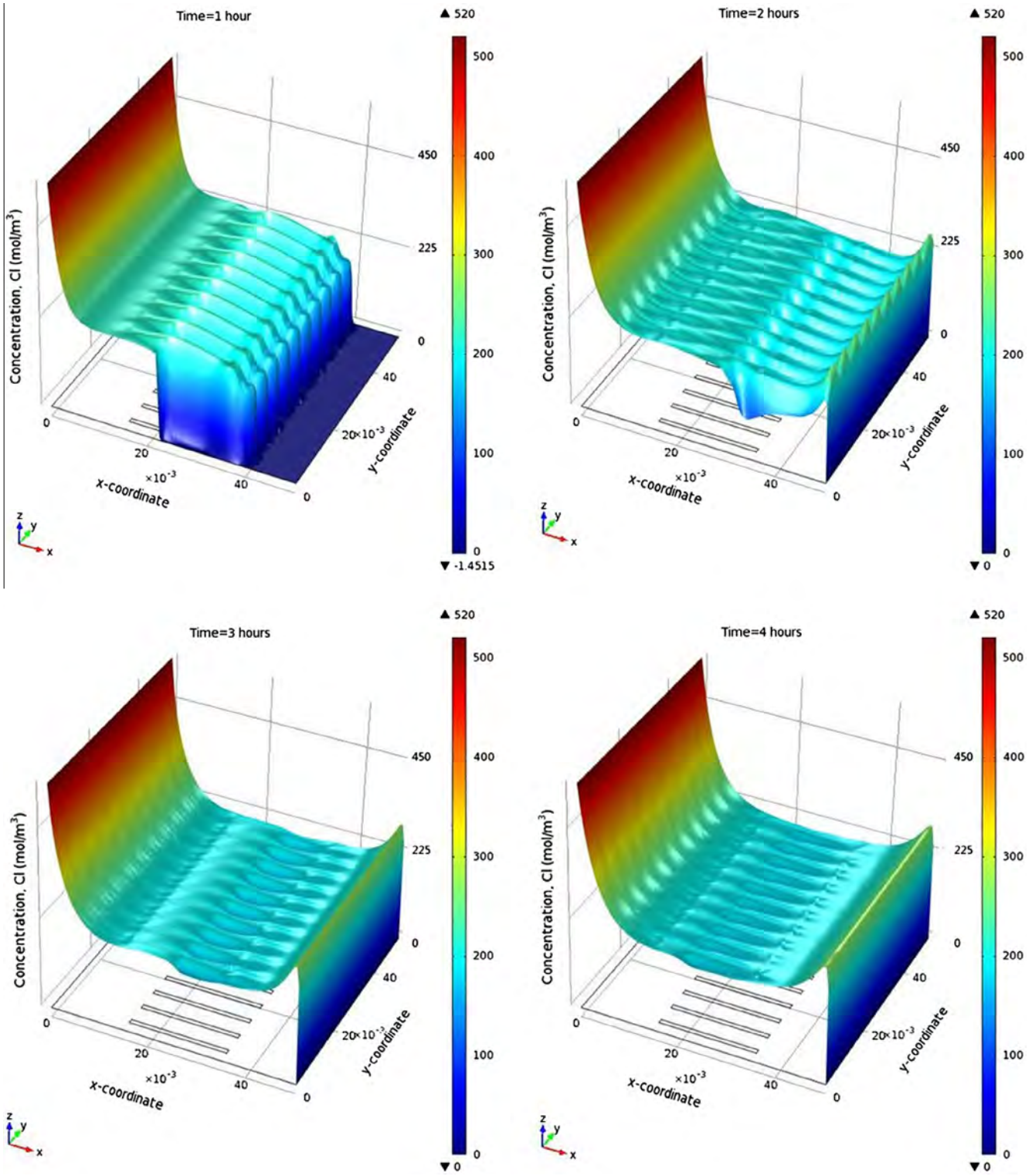

Fig. 9. Concentration distribution profiles of chloride ions.

creates an internal electrostatic potential which can affect the transport of all ionic species in the concrete throughout the time and space. This electrostatic potential increases with the externally applied electric field and the difference of diffusivities between ionic species. In order to accurately describe the internal charge imbalance between different species and also achieve the true multi-species coupling, recent work [28–32] suggested that one should use the following Poisson's equation to govern the electrostatic potential in the transport medium,

$$\nabla^2 \Phi = -\frac{F}{\varepsilon_0 \varepsilon_r} \sum_{k=1}^{N} z_k C_k \tag{6}$$

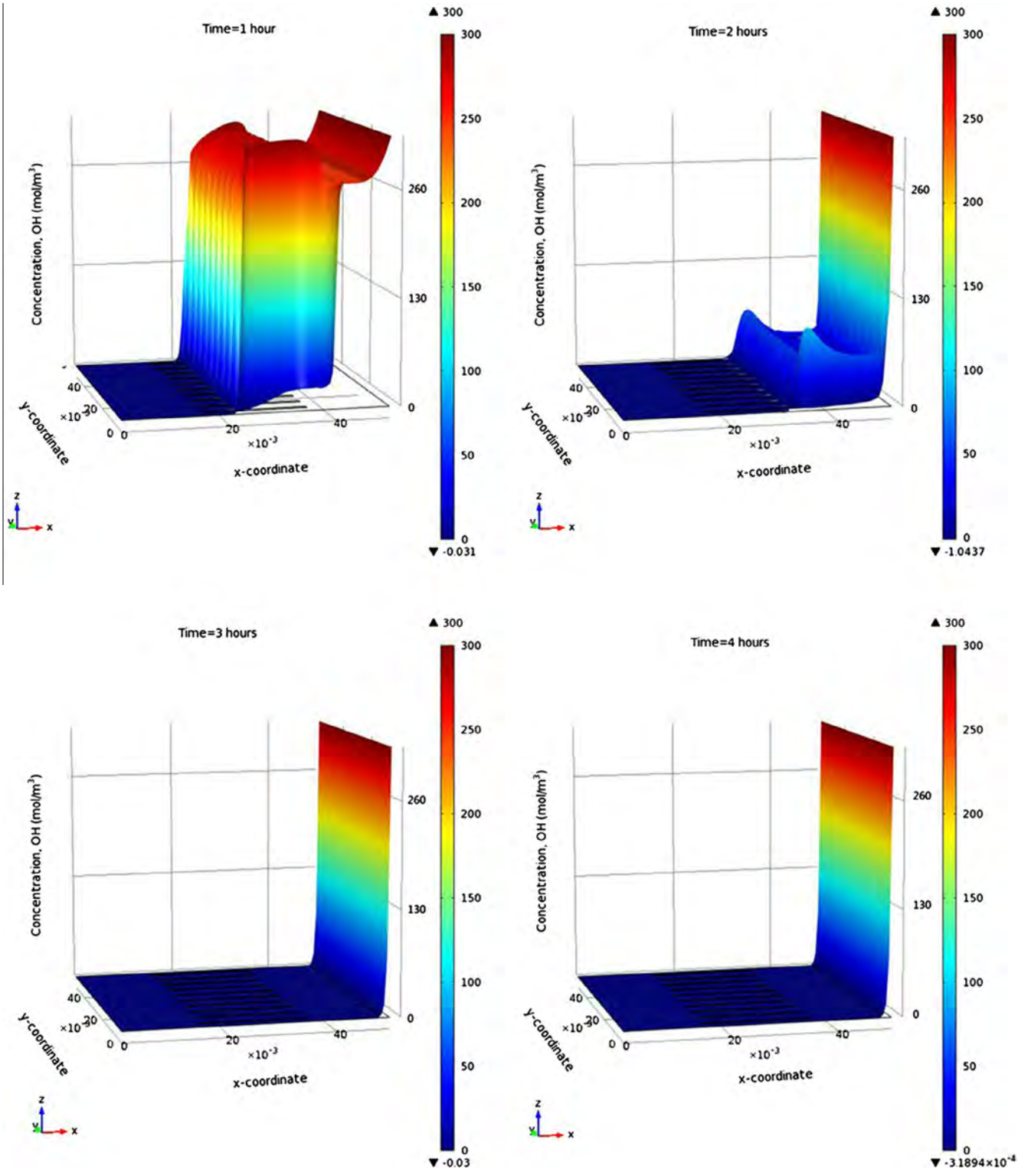

Fig. 10. Concentration distribution profiles of hydroxide ions.

where $\varepsilon_0 = 8.854 \times 10^{-12}\,\mathrm{CV^{-1}\,m^{-1}}$ is the permittivity of a vacuum, $\varepsilon_r = 78.3$ is the relative permittivity of water at temperature of 298 K, and N is the total number of ionic species involved in the solution. For numerical modelling, the use of Poisson's equation creates two difficulties. One is the coupling of Eq. (5) between different ionic species, since Φ is now dependent on not only the boundary conditions defined by the externally applied electric field, but also the concentrations of all ionic species involved in the medium. The other is the nonlinearity and numerical difficulty which involves calculations of large and small numbers that need be handled carefully [31,32]. Nevertheless, Eqs. (5) and (6) can be used to determine the electrostatic potential, Φ, and the concentrations of individual ionic species, C_k ($k = 1,2,\ldots,N$), at any time and any point in the solution domain, provided that the initial and boundary conditions are properly defined.

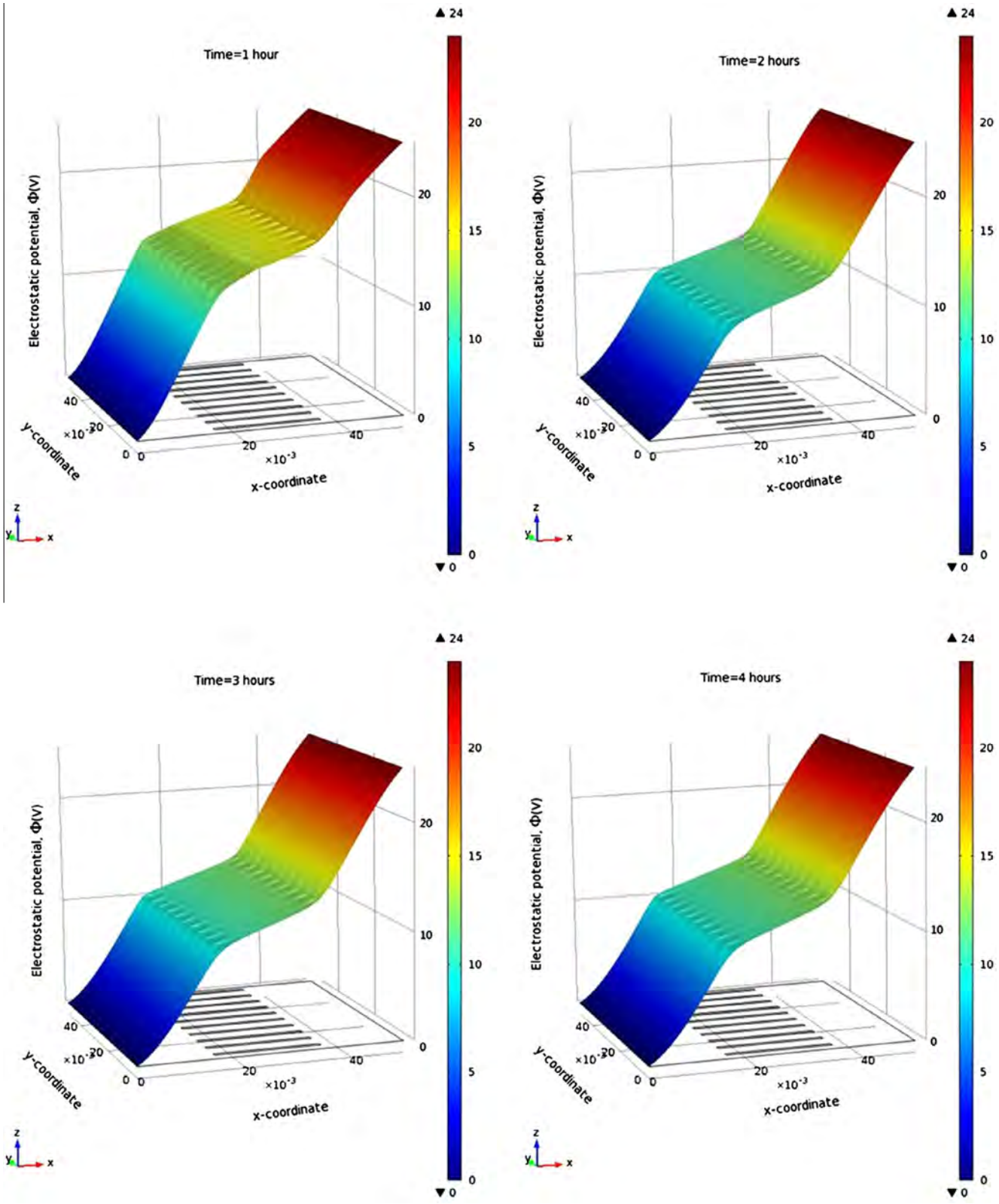

Fig. 11. Electrostatic potential distribution profiles.

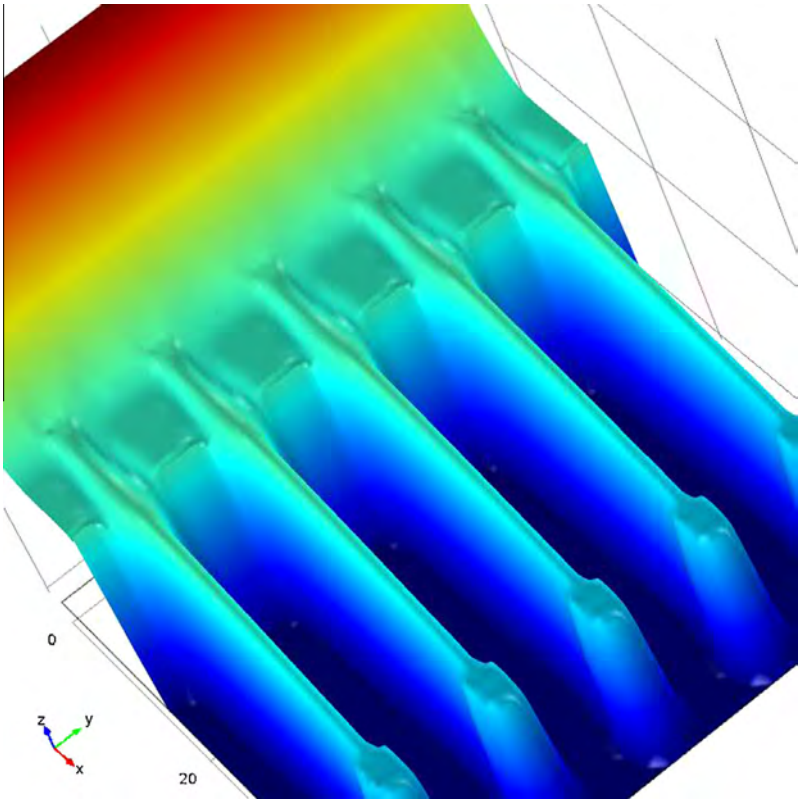

Fig. 12. Zoomed-in schematic for 'shock waves'.

3. Multi-component transport models for heterogeneous concrete with mesocrack

3.1. Modelling

A set of 2-D mesoscale cracked concrete geometries with a mesocrack are developed to simulate the RCM tests. The concrete modelled here is treated as a heterogeneous composite structure with three phases consisting of mortar matrix, coarse aggregates and ITZs. Fig. 1 shows one of the models adopted in this simulation, in which the circular areas represent the impermeable aggregates with the radii ranging from 1.5 mm to 10 mm. These aggregates are randomly generated in a certain volume fraction ($V_a = 0.5$ in Fig. 1) in the geometry by using MATLAB software. Note that though the shape of aggregates may not be such perfectly circular in reality and the particle shape may cause influence on the transport properties of concrete in 3-D to some degree [25,48], it only makes a modest influence for a 2-D aggregate distribution according to the previous studies [18,46,49]. Outside each aggregate, there is an aureole ITZ shell wrapping the aggregate. Note that the real thickness of ITZs in normal concrete is only 20–50 μm [50,51]. However, this kind of thin layer creates some difficulty in the element mesh of ITZs due to the computing limitation; therefore, the ITZ layer in the present model is artificially increased to 100 μm. In order not to overestimate the ITZ effect, the increase of ITZs volume in the present model is compensated by the reduction of the diffusion coefficients of ions in the ITZs. Outside the ITZs, the remaining part of the concrete model represents the mortar matrix. A single mesocrack located near the edge of the concrete was created based on the same principle as used in the fracture modelling [18,19]. The width and length of the crack were assumed but the shape was generated following a weak-link of the material in that region. The crack starts on the edge ($x = 0$) and its width is assumed to be twice the thickness of the ITZs.

Fig. 2 shows the finite element mesh used in this heterogeneous model. As the aggregates (white area) are assumed to be impermeable, they are not meshed in the model, which means that the ionic transport takes place only in the mortar (blue[1] area), ITZs and crack (black area), although the diffusion coefficients are different in these domains. The continuous conditions are assumed for both concentration and flux at the interface between the different domains. Note that, the accuracy of the numerical solution of the convection–diffusion equation governed by Eqs. (5) and (6) is highly dependent on the element sizes used. Mathematically, for finite element analysis, to achieve a reasonably accurate numerical solution, one has to make local Peclet number (defined by the ratio of the diffusion time h^2/D to the convection time h/u, where h is the element size, u is the convection velocity, and D is the diffusion coefficient) to be less than one [31,32]. Hence, the larger the convection velocity, the smaller the element size required. In the present problem, the convection velocity is the migration velocity of ionic species. When there is an external electric field, the transport of ions in the electrolyte is usually dominated by the migration. In this case the element size must be very small. Otherwise, the numerical solution obtained might not be convergent or inaccurate.

For the concrete modelled herein, the transport parameters employed for different phases are listed in Table 1. Since the crack width assumed in the presented model is larger than 100 μm, the ionic diffusivity in the crack (D_C) is taken as 60 times of that in the bulk mortar (D_B) [17]. The larger value of D_C is probably because, in microscope scale, the cracks increase the connectivity between capillary pores and ITZs within the damage region. In terms of

[1] For interpretation of colour in Fig. 2, the reader is referred to the web version of this article.

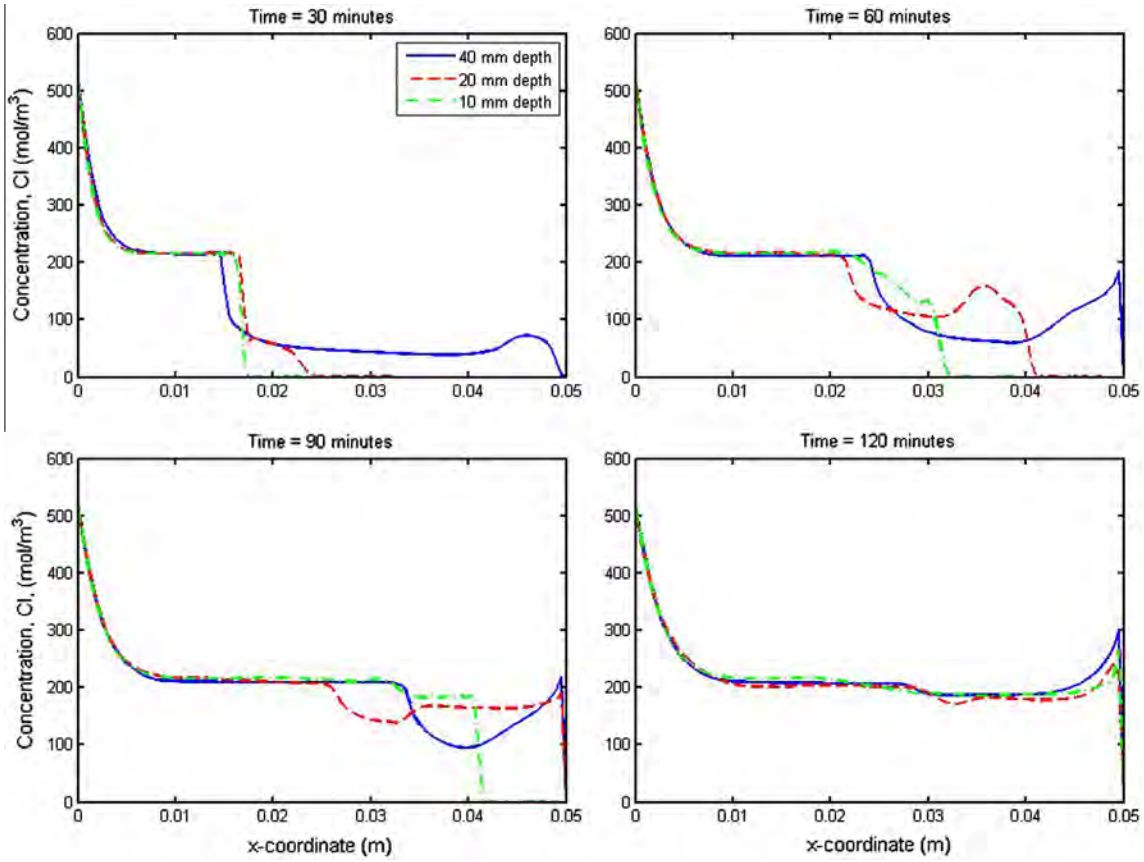

Fig. 13. Comparisons of average *y*-axis concentration distributions between three models (different depths).

the transport property of ITZs, existing data showed that the ratio of diffusion coefficients between ITZs and matrix is about 4–15, depending on the porosity and water-to-cement ratio of individual specimens [52–54]. Considering the use of large thickness of ITZs in the present models, the diffusion coefficient in ITZs for each ionic species employed in the present study is taken as three times of that in the bulk mortar.

The model described above is used to simulate the RCM test of concrete, in which the 50 mm × 50 mm plain concrete specimen is located between two compartments, one of which has a 0.52 mol/l NaCl solution, the other of which has a 0.30 mol/l NaOH solution. An external potential difference of 24 V is applied between two electrodes inserted into the two compartment solutions. The ionic species to be analysed in the simulations include potassium, sodium, chloride and hydroxyl. Note that other ionic species (such as calcium and sulphate) may also exist in the concrete. However, owing to their low concentrations they are not considered in the present simulations. Fig. 3 graphically displays the simulated test. Also, since the volume of either compartment is much greater than that of the specimen, it is reasonable to assume that the concentrations of each ionic species in the two compartments remain constants during the migration test. Table 2 shows the initial and boundary conditions employed in the present study. Note that the boundary settings here are different from those used by Šavija et al. [18] (in their work the upstream Dirichlet boundary conditions are applied not only at the left boundary of concrete but also inside the domain of the crack), though the relevant geometries of the two studies are very similar. In the present model, for the sake of efficiently exploring the differences between multi- and single-component migrations in the region subjected to concrete cracks, the crack herein is treated as a new meso-scale phase for ionic transport, rather than an exposed boundary as utilised in [18].

3.2. Comparisons between multi- and single-component models

For given initial and boundary conditions, Eqs. (5) and (6) are solved numerically by using commercial software COMSOL. Concentrations of four ionic species and the electrostatic potential distributing in the cracked concrete during the migration test can be obtained. For the purpose of comparison between the multi-component and single-component models, another simulation using the same governing equations but with the assumption of electro-neutrality condition (i.e. the Laplace equation $\nabla^2\Phi = 0$ is used to replace the Poisson's equation) is also performed. The comparisons between the two models for the electrostatic potential and chloride concentration are shown in Figs. 4 and 5, respectively.

In the 3-D plot shown in Fig. 4, the two plane coordinates represent the position of the variable in the 2-D concrete and the vertical coordinate is the value of the variable, i.e. the electrostatic potential. It can be clearly seen from the profile of single-component model that, the electrostatic potential does not change with time. Moreover, as indicated by Laplace equation, if the electro-neutrality condition holds, the electric field would be time-independent, which is in agreement with what is shown in Fig. 4b: i.e. electrostatic potential increases from $\Phi = 0$ at the cathode to $\Phi = 24$ V at the anode and the increase is almost linear. The local fluctuations in the profile are due to the heterogeneous nature (e.g. the presence of aggregate phase). In contrast, the electrostatic potential profiles predicted by multi-component model show some different features. When the transport process is controlled by Poisson's equation, the electrostatic potential increases also from $\Phi = 0$ at the cathode to $\Phi = 24$ V at the anode, but the increase seems not linear (see Fig. 4a). Interestingly, there is a convex shape occurring in the distribution profile and this convex shape gradually moves along *x*-axis. A careful examination shows that the

movement of the convex shape is generally in accordance with that of chloride migration wave front in the bulk mortar. This means that, initially the higher migration speed of ionic species is in the region near the cathode, but with the increase of time it gradually shifts to the region near the anode. Hence, the electrostatic potential gradient in the multi-component transport model is not constant but time and regionally dependent. Note that the crack added in the models seems to have very little effect on the electrostatic potential. This is likely because the electrostatic potential is mainly dependent on the externally applied electric field and the difference of diffusion coefficients between different ionic species. In the present examples, the diffusion coefficients are proportionally increased in the crack zone and thus their relative values remain unchanged.

Obviously, different electrostatic potential distributions will generate different ionic transport features. It can be noticed from Fig. 5 that, though the chlorides give priority to penetrate in the mesocrack in both models but their travel speeds are quite different: the migration speed shown in the multi-component model is much higher than that shown in the single-component model. By a more careful check on the results of the two models, one may observe that, the concentration in the multi-component model drops sharply in the region near the cathode due to the combined actions of boundary conditions and multi-species coupling, whereas the concentration in the single-component model drops gradually from the upstream edge to the region where the chlorides have arrived. Furthermore, it can be seen from Fig. 5a that the chlorides have a perfectly uniform concentration distribution in both the mesocrack and mortar, as well as have a clear integral migration wave front characterised by the abrupt change of the colour legend in the interface between chloride and chloride-free regions. In contrast, this phenomenon does not appear in the results shown in Fig. 5b, where the chlorides simply more gather in the region more near the upstream edge and the presence of the mesocrack does not make notable impact on the chloride transport. To sum up, the multi- and single-component models have totally distinct transport features, not only for the electrostatic potential distributions but also for the chloride penetration behaviours. Therefore, considering the ionic interaction in transport models to predict chloride penetration in concrete with cracks is very important, as demonstrated previously in concrete with no cracks [28–32,35,55].

4. Multi-component transport models for homogenous concrete with damage zones

4.1. Modelling

In the previous section, the significance of multi-species ionic interactions governed by Poisson's equation has been demonstrated. In order to further investigate the mechanism of ionic transport in the concrete with multiple cracks, this section makes two changes on the previous geometric models, aiming at easier observation of the concentration profiles. Firstly, a set of simplified concrete geometries are modelled, in which all aggregates and ITZs are removed from the previous three-phase model. Secondly, the cracks are represented by the large scale "damage zones". Note that the concept of "damage zone" has been widely used in damage mechanics to simulate the overall effect of cracks on the mechanical performance of concrete materials [56]. This concept has been recently introduced into the chloride transport problems by Bentz et al. [17]. They proposed an imaginary zone consisting of 'damage mortar', which surrounds each crack. This kind of zone is

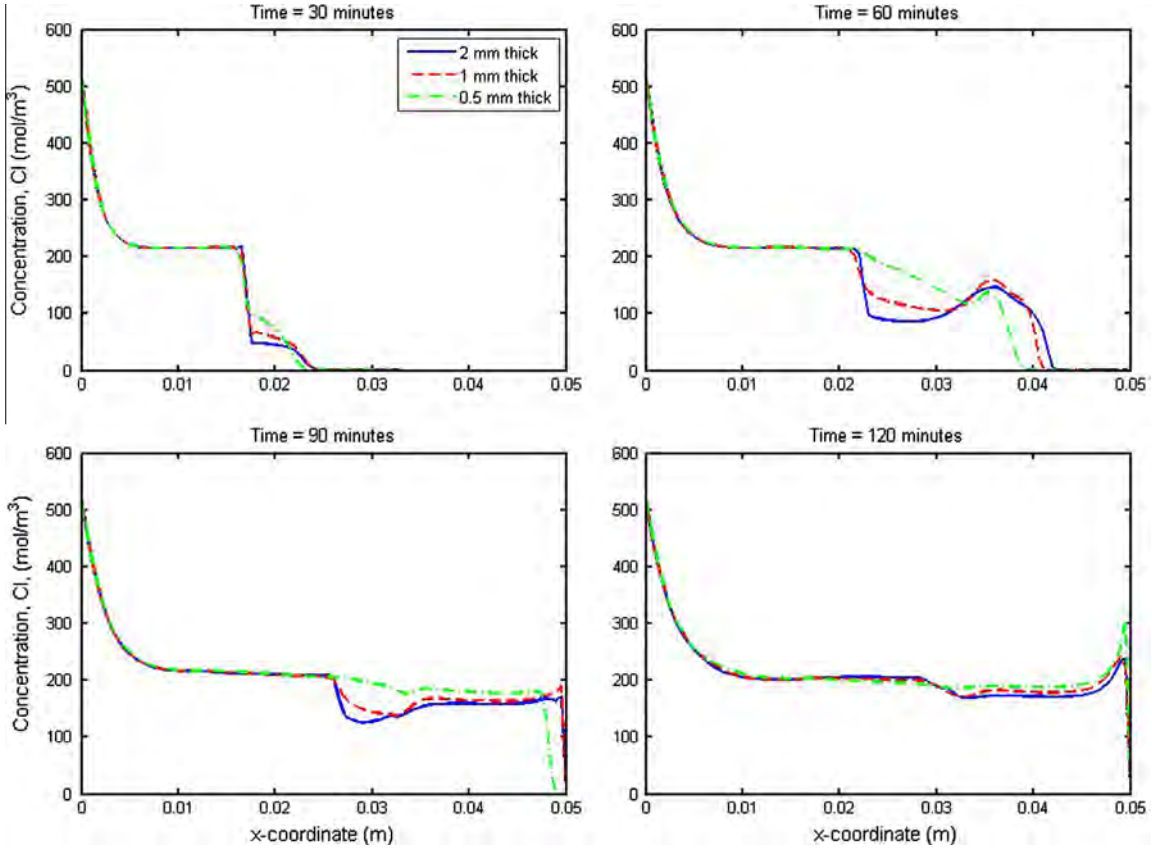

Fig. 14. Comparisons of average *y*-axis concentration distributions between three models (different widths).

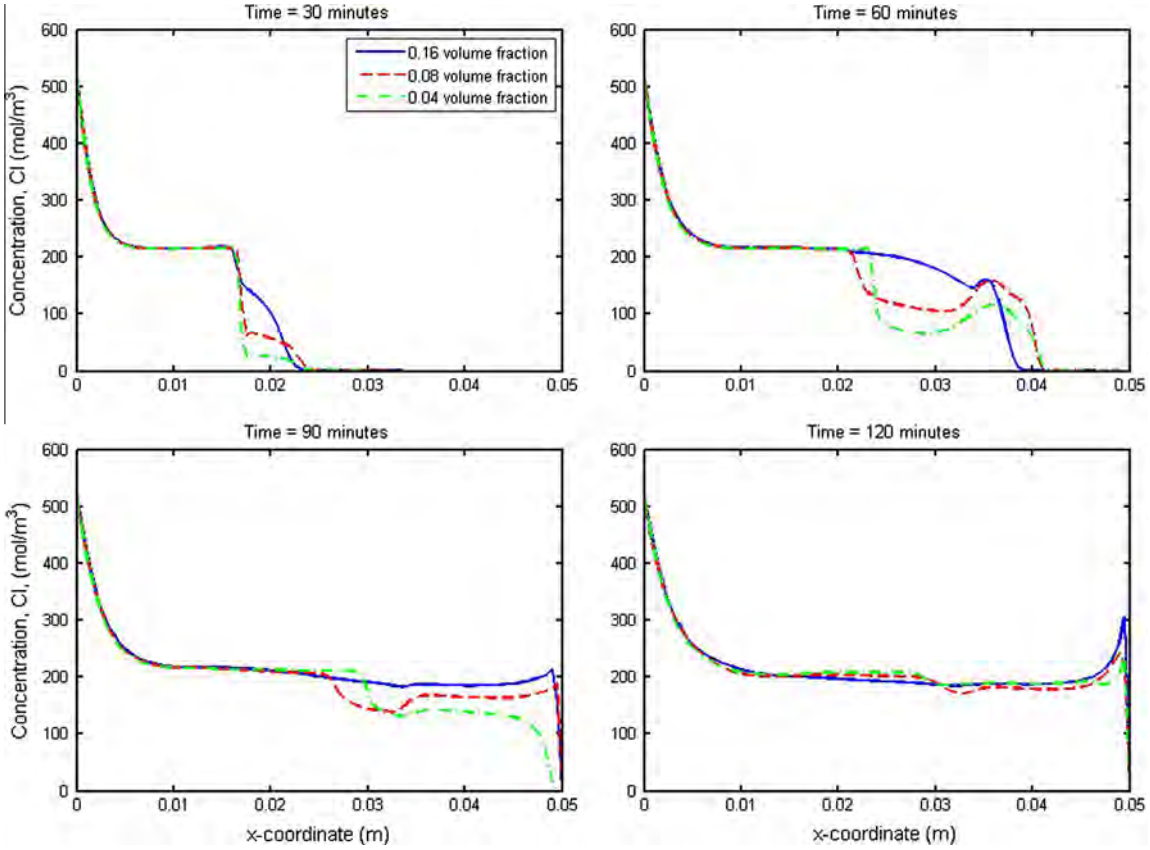

Fig. 15. Comparisons of average *y*-axis concentration distributions between three models (different damage fractions).

about 1–4 mm width, in which the diffusion coefficient is smaller than that in cracks but larger than that in bulk mortar. The width of a damage zone depends on the width of the central crack itself. To introduce this type of damage zone into the present model, two hypotheses are made herein. Firstly, due to the small width of central crack, the multi-phase structure of damage zone in the present model is ignored. That is the damage zone including the central crack is simplified as a single phase and assumed to be uniform. The ionic diffusion coefficient in the damage zone, D_D, is taken as 20 times higher than that in the bulk mortar (D_B) according to [17]. Secondly, all damage zones in 2-D geometry are assumed to be ideally rectangular in shape and can be characterised by their individual width and length, which is similar to what was used by Bentz et al. [17]. Note that although the micro pore prosperities such as constrictivity, tortuosity and connectivity make the cracks display a complex 3-D geometry, one can still simplify the problem from 3-D to 2-D with suitable definitions on crack width and depth.

In consideration of that most of existing cracking models only focus on a single crack and the adjacent cracks are probably assumed to be sufficiently far away from each other [13–18], the present model is also to examine the interactive effect caused by the multiple damage zones. Fig. 6 shows the geometries of concrete with different patterns of damage zones, in which all of the damage zones are assumed to be in a rectangular shape and have identical width (1 mm) and volume fraction ($V_D = 0.08$) but different lengths. The damage zones are located in the middle of the concrete. This represents the case where a cracked concrete has been repaired on its surface but the cracks or damage inside of the concrete remains. For the convenience of examination, all damage zones in each individual case are identical and parallel to the transport direction.

Similar to the models presented in the preceding section, the above geometries are used to simulate an eight-hour RCM test, the set-up of which is the same as that shown in Section 3.1 (Fig. 3). The transport properties of different phases, boundary and initial conditions used in this section are defined also in Tables 1 and 2, respectively.

4.2. General view of migration results

As the heterogeneous nature of the concrete has been ignored (coarse aggregates and ITZs) in the models, one can receive a more clear view focusing on the concrete damage zones from the

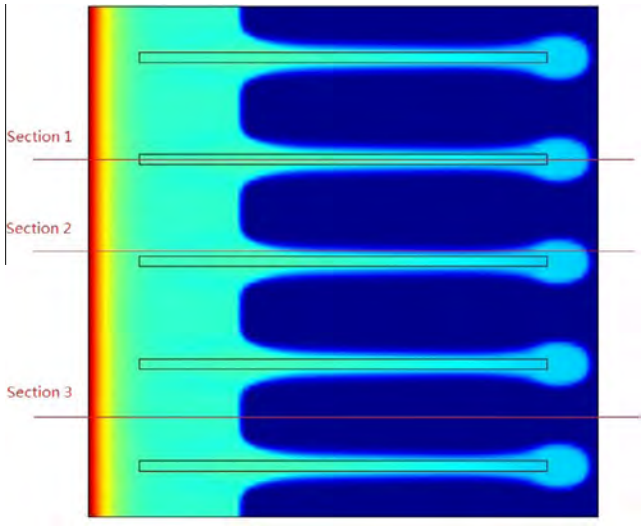

Fig. 16. Schematic view for three cross sections traversing the simulated specimen.

simulation. Again the mass conservation equations and Poisson's equation are solved numerically. Figs. 7–11 display the distribution profiles of five variables (concentrations of four ionic species plus one electrostatic potential) at four different times during the first 2 h obtained from one of the models, in which there are ten damage zones, each with 1 mm width, 20 mm length, and 0.08 volume fraction. It is clear from the figures that, the present profiles are significantly different from those obtained from the uncracked concrete models [32]. As is to be expected, the migration wave fronts travel at two distinct rates. One occurs in the part with no cracks and its speed is similar to that observed in the uncracked concrete model; the other occurs in the damage zones with a much higher travel speed, which is similar to what was observed in the chloride profiles obtained from a cracked concrete subjected to wetting–drying cycles [5]. This appears to be expected as the wetting–drying cycles produce a convection flow to ions, which is similar to the migration of ions.

Some interesting features are found from the ionic distribution profiles in the high speed zones. Fig. 12 shows the zoom-in plot of one of the ionic wave fronts. It can be seen from this plot that the high speed zone is somehow spread from the damage zones, particularly in the wave front, where there is an elliptical aggregation of ions around each wave front and the size of the short axes of the ellipse aggregation is approximately as 2–4 times the width of a damage zone. More figuratively speaking, the concentration distribution along the damage zone presents a 'dumbbell shape', which is vividly demonstrated in Fig. 12. The formation of this kind of 'dumbbell shaped distribution' is likely due to the diffusion coefficient gradient. The ion gives priority to travel in the direction which has larger diffusion coefficient: around the middle part of a damage zone, since the neighbouring region is still damage, the ions tend to only migrate along the x-axis (along the damage zone), acting like a laser beam; whereas around the end of a damage zone, since it has the same diffusion coefficient (all bulk mortar) in each adjacent direction, the ions are thus dispersed. Therefore, the average y-axis concentration in the sections of the end of damage zones (e.g. the section of $x = 0.045$ m of the solid line in the upper left figure of Fig. 13) becomes larger than those in the sections of middle part of cracks (e.g. the sections from $x = 0.025$ m to $x = 0.04$ m of the solid line in the upper left figure of Fig. 13) to some extent.

4.3. Sensitivity analysis

To understand the influence of cracking-induced damage zones (e.g. widths, lengths and volume fractions of damage zones) on chloride migration, a series of sensitivity analysis are carried out. In Figs. 13–15, the average y-axis concentration distributions during the first 2 h process are clarified by three categories: the models reported in Fig. 13 have the same damage width (1 mm) and fraction ($V_D = 0.08$), but different damage lengths (e.g. 10 mm, 20 mm and 40 mm); the models reported in Fig. 14 share the same damage length (20 mm) and fraction ($V_D = 0.08$), but different damage widths (e.g. 2 mm, 1 mm and 0.5 mm); the results shown in Fig. 15 are calculated from three models which contains the distinct numbers of cracks ($V_D = 0.04$, 0.08 and 0.16) but the same size of an individual damage zone (1 mm width and 20 mm length). By examining the locations of migration waves and the peak values of concentration in the migration waves, it is concluded that the damage length dominates the migration rate, whereas the damage width has little influence on the chloride migration. This finding agrees with the previous single-component models [17,18]. Additionally, in terms of the models with the same length of damage zones, the chlorides will also achieve more rapid migration rate

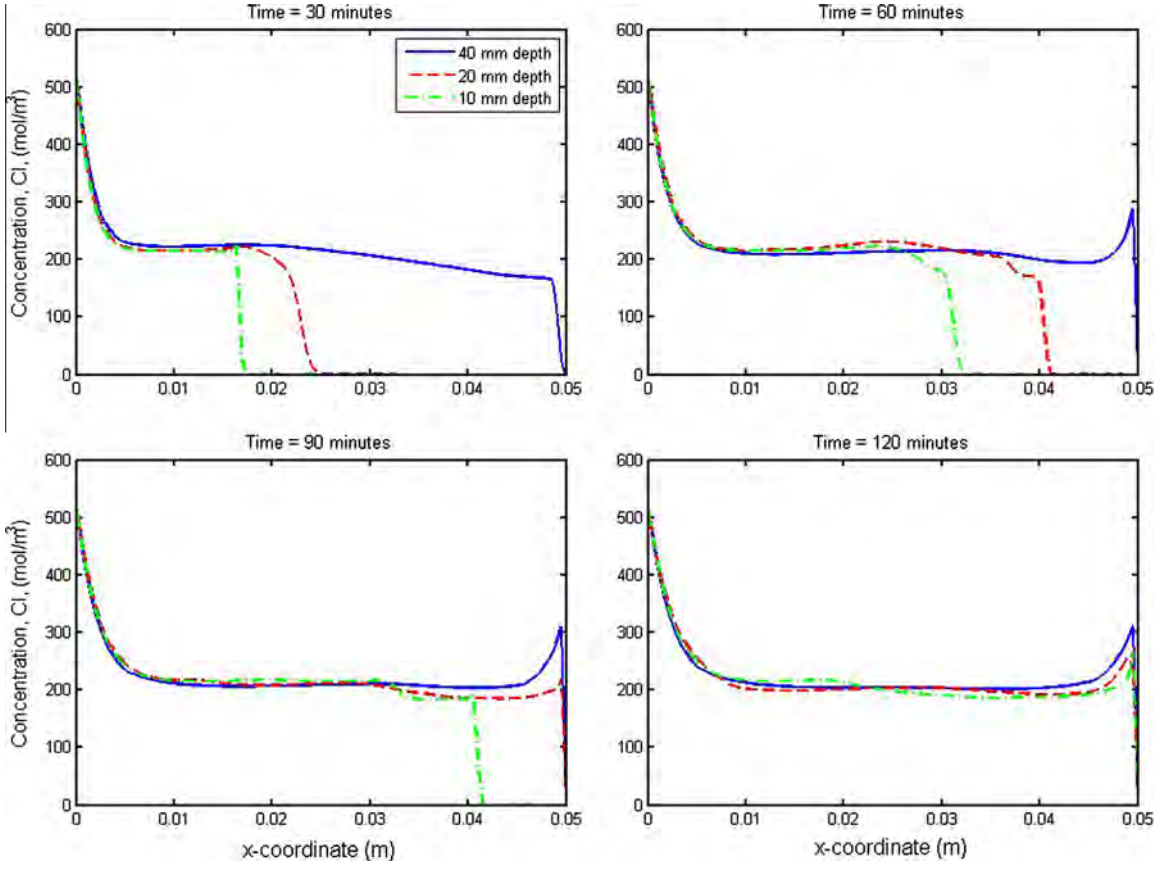

Fig. 17. Comparisons of concentration distributions in Section 1 between three models (different depths).

in the model that has a larger damage volume fraction even this effect is not as evident as that of the damage length.

One may argue that the use of average y-axis concentration profiles is difficult to distinguish the quantitative distributions between the areas of the damage zones and the bulk concrete. To deal with this issue, three categories of cross sections traversing the simulated specimen were selected. As shown in Fig. 16, the first section is the centre line of one damage zone. The second section represents the cut line near the damage zones, intersecting the elliptical aggregation of ions at the wave fronts. The third section is located evenly between two damage zones, where the farthest section is from any damage zones. Looking at these three specified sections, one can re-plot and obtain a more visualized view of the sensitivity analysis on the properties of cracked concrete than those shown in Figs. 13–15.

4.3.1. Lengths of damage zones

Figs. 17–19 show the comparison of chloride concentration distributions during the first 2 h process along the three different sections in the models with the different damage lengths as noted previously. Fig. 17 clearly demonstrates how the damage depth dramatically accelerates the migration rate; the concrete specimen including 40 mm length damage zone is much more quickly permeated by the chloride ions. It is apparent from Fig. 18 that the chloride migration rate is also markedly influenced by the damage length in the region near the damage zones, due to the intersection between the cut line of Section 2 and the elliptical aggregation of ions around wave front.

However, when it comes to the third section (non-damage area of concrete), the situation changes greatly; the concentration profiles seem to be irregular, especially those in the model with 20 mm and 10 mm length damage zones. With regards to this phenomenon, since in this case the three models have the same damage width and volume fraction, the model with 20 mm and 10 mm length damage zones have the larger amount of cracks, which leads the space between two adjacent damage zones to be narrower. As is shown in Fig. 12, during the migration process, the chloride concentrations in the damage zones are higher than those in the neighbouring bulk mortar and thus the diffusion behaviour of chlorides occurs. Generally speaking, this kind of 'pollution' due to local diffusion could produce the disordered concentration distribution profiles, which is illustrated in Fig. 19. This phenomenon apparently shows the interactive effect caused by dense array of multiple cracks and it cannot be found in the concrete model with only a single crack.

4.3.2. Widths of damage zones

Likewise, the chloride concentration distributions focusing on the effect of different damage widths are re-plotted in Figs. 20–22 based on the three sections of interest. Comparing Figs. 17 and 20, it is evident that, under the same changing multiplier, the influence of damage width is much smaller than that of damage length. When the damage width is doubled, it only leads to a tiny increase in progress to the chloride penetration. This feature is reflected in the profiles in the second section (Fig. 21). Approximately, one may find that both the migration wave fronts taken place in bulk mortar and the wave fronts around the end of damage zones have the same travel speed. Similarly with the phenomenon displayed in Fig. 19, the 'pollution' behaviour due to local diffusion caused by dense array of multiple cracks again disrupts the discipline of concentration distribution profiles along the non-damage area of concrete; that is the number of damage zones, instead of the damage width, which dominants the chloride migration in non-damage section. Note that if the cracks are very small the width of cracks

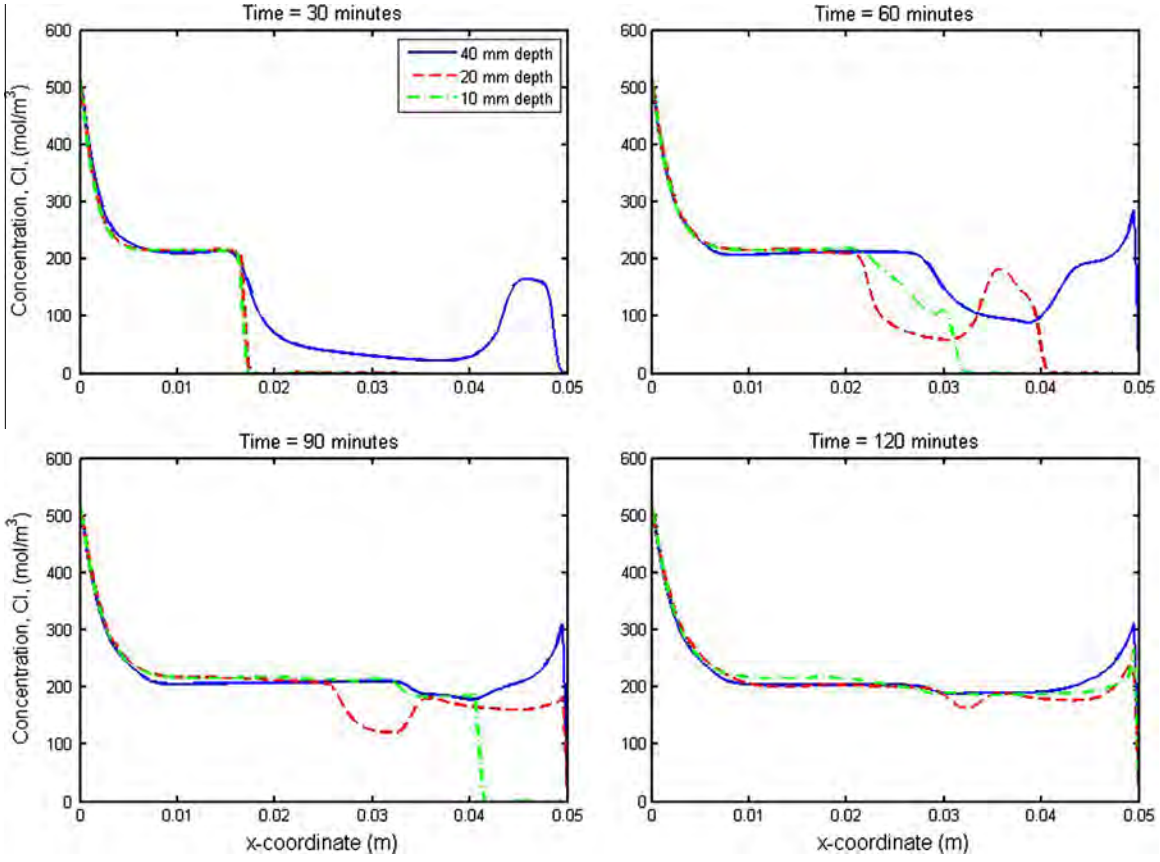

Fig. 18. Comparisons of concentration distributions in Section 2 between three models (different depths).

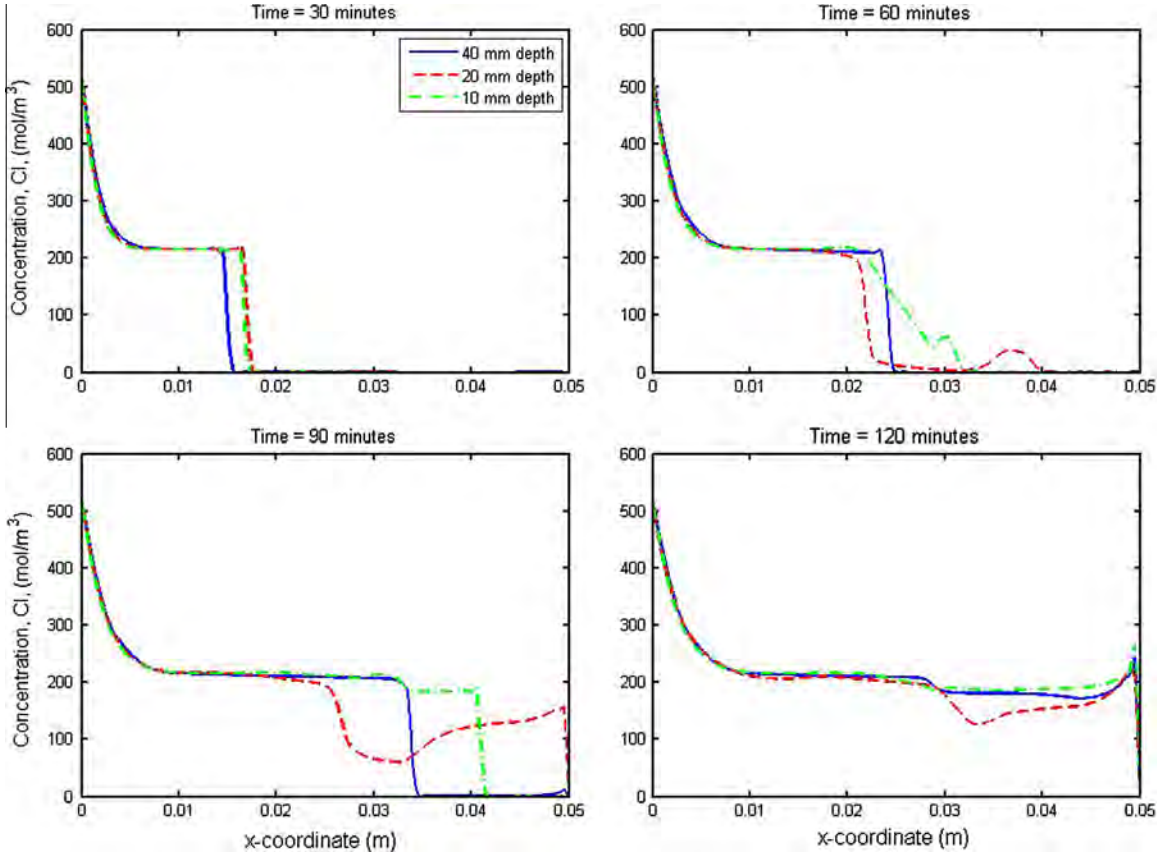

Fig. 19. Comparisons of concentration distributions in Section 3 between three models (different depths).

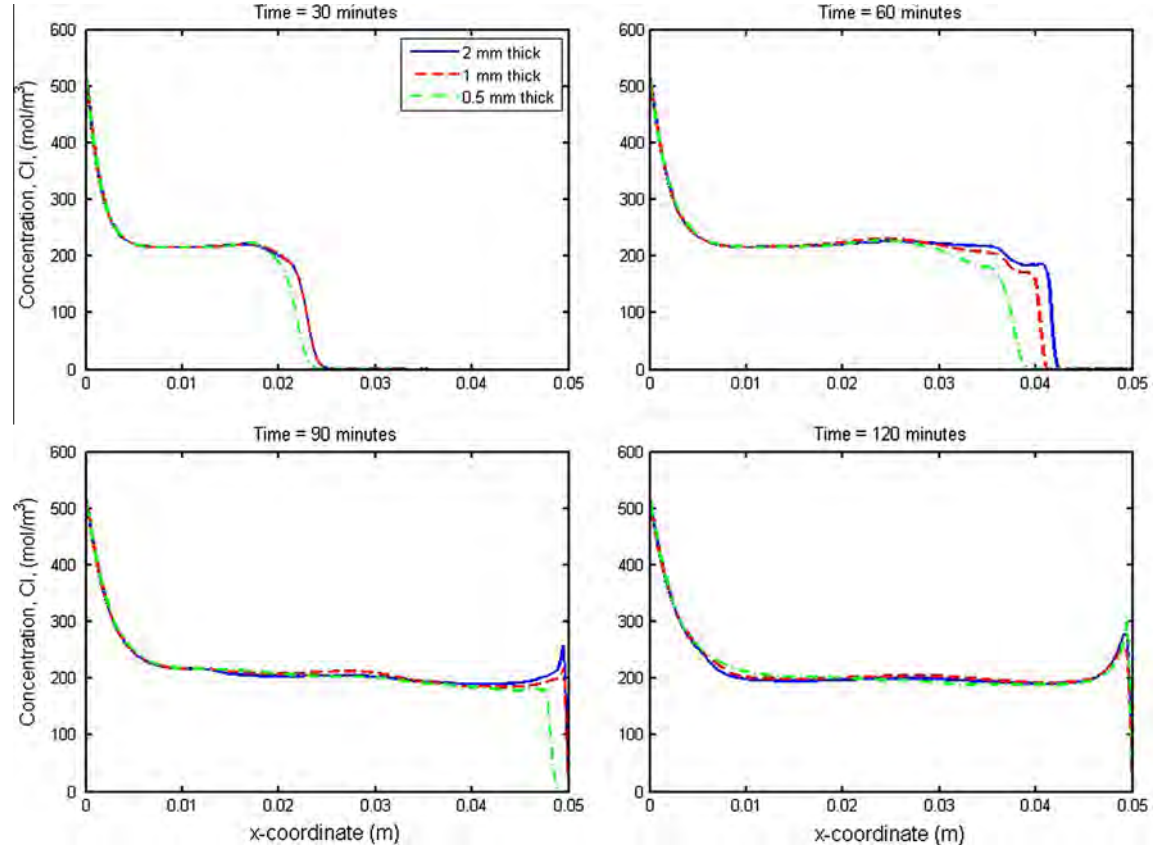

Fig. 20. Comparisons of concentration distributions in Section 1 between three models (different widths).

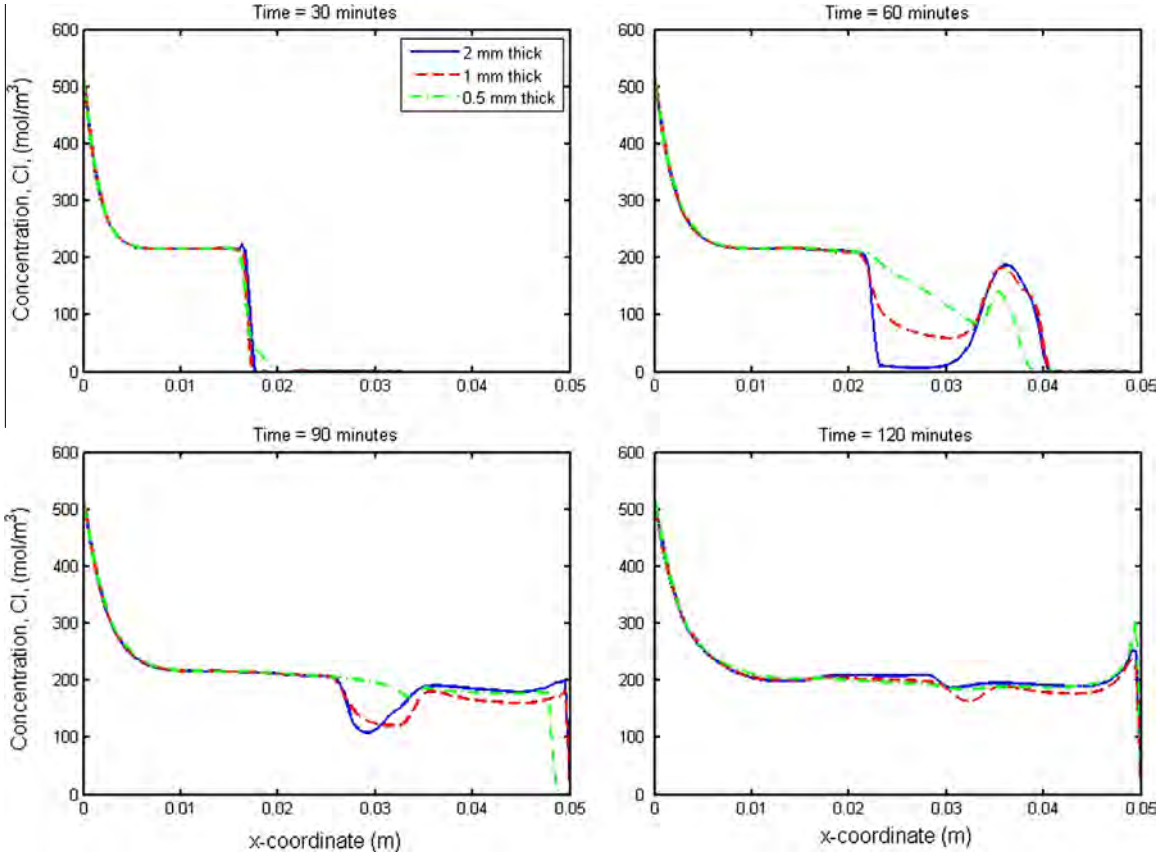

Fig. 21. Comparisons of concentration distributions in Section 2 between three models (different widths).

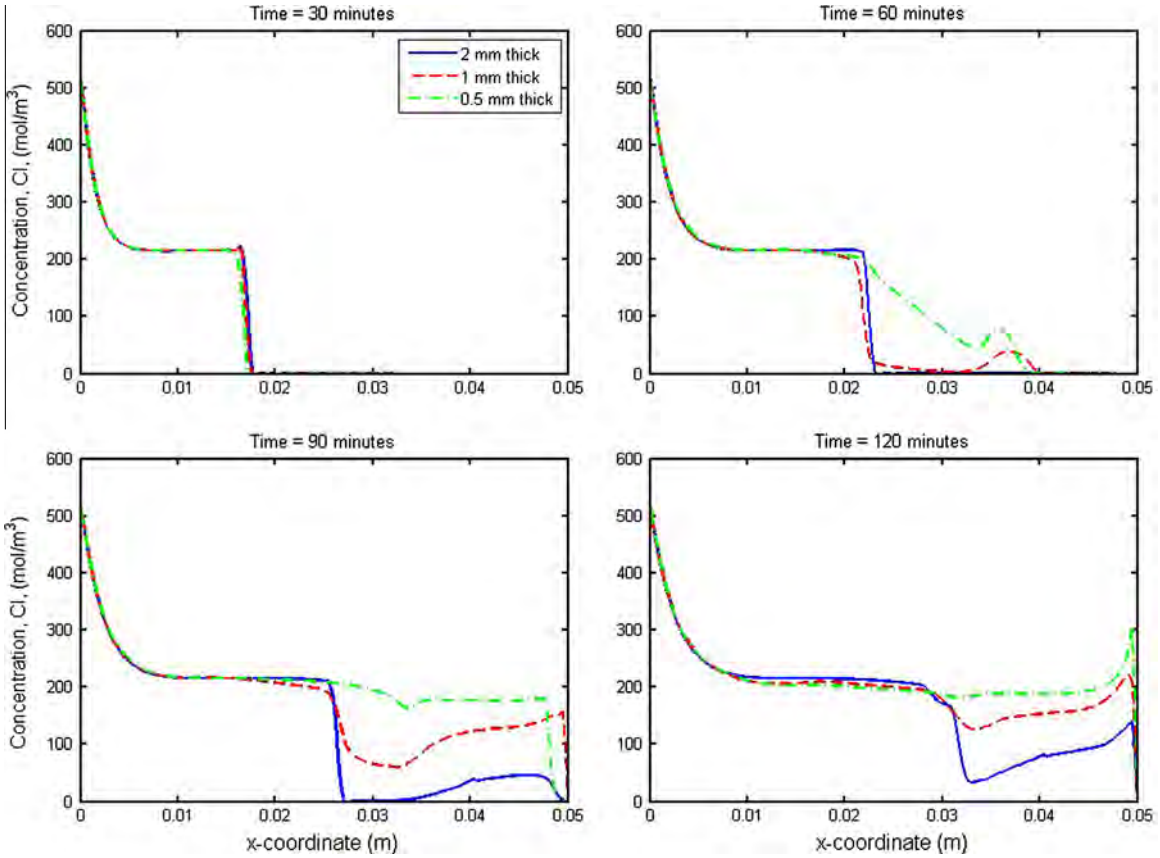

Fig. 22. Comparisons of concentration distributions in Section 3 between three models (different widths).

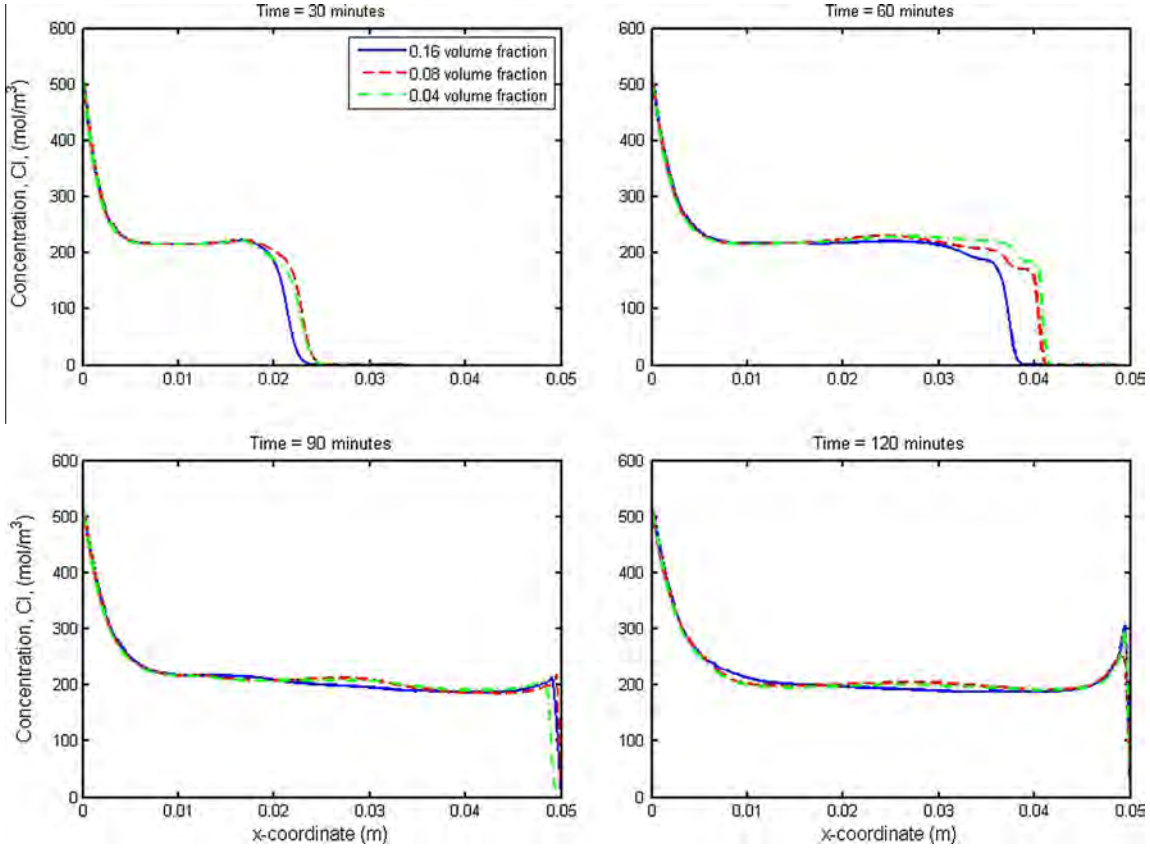

Fig. 23. Comparisons of concentration distributions in Section 1 between three models (different damage fractions).

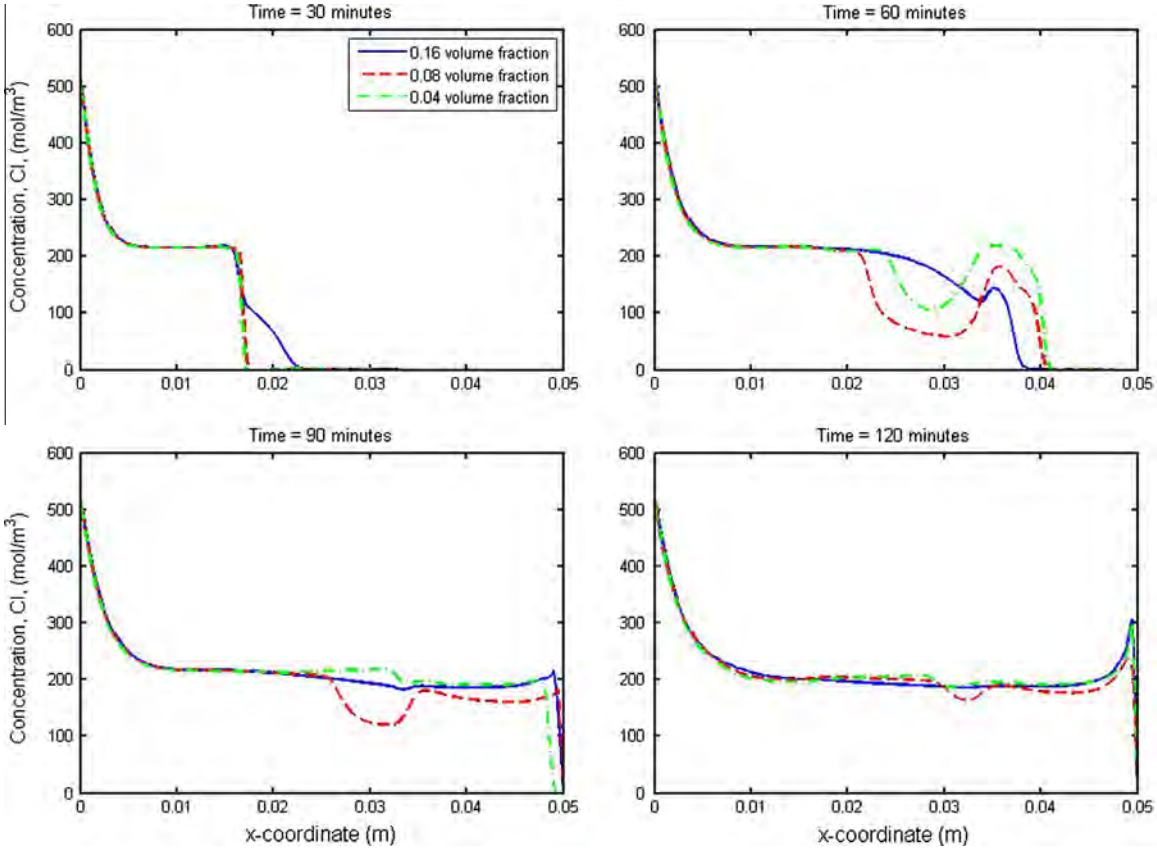

Fig. 24. Comparisons of concentration distributions in Section 2 between three models (different damage fractions).

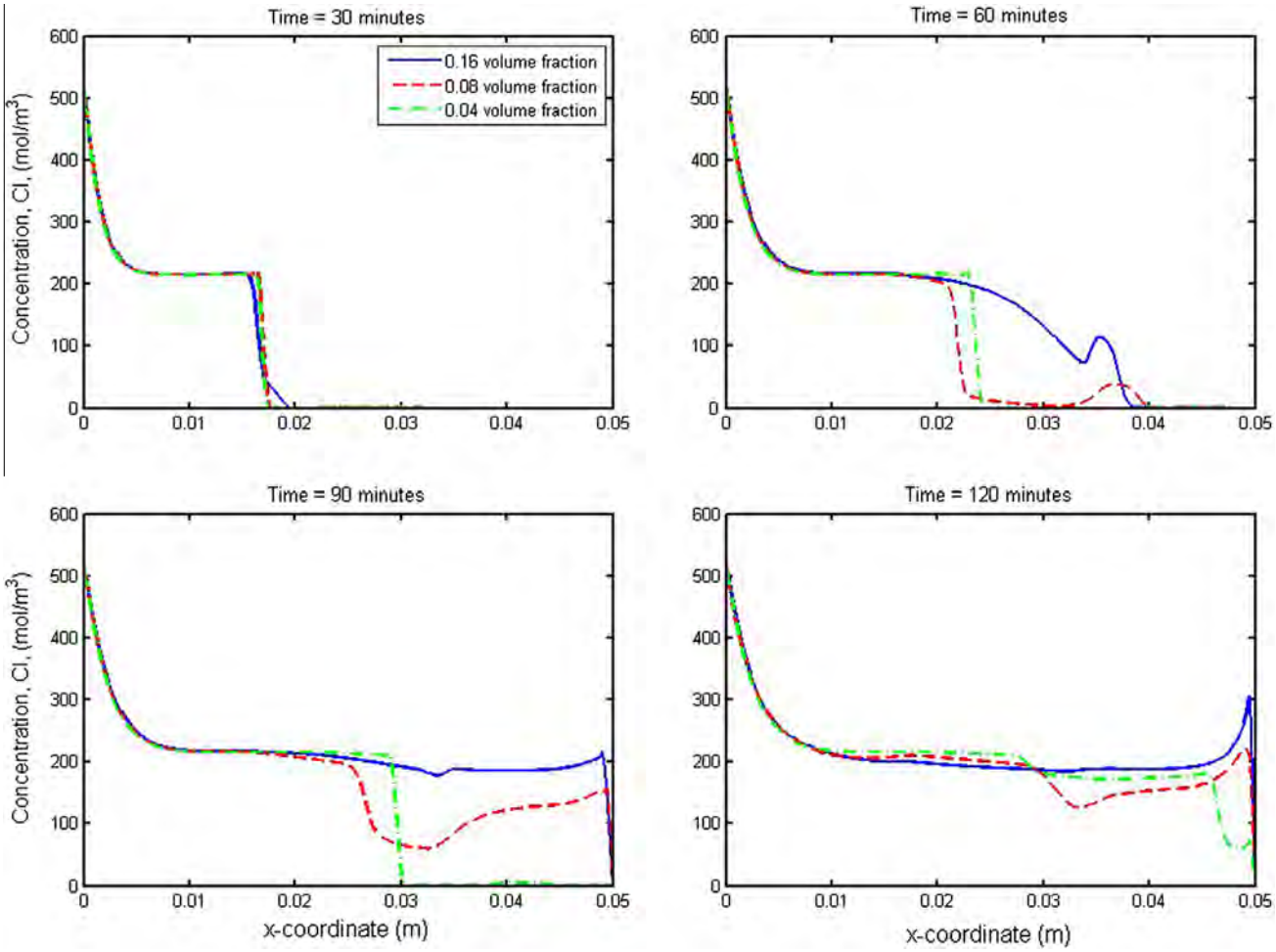

Fig. 25. Comparisons of concentration distributions in Section 3 between three models (different damage fractions).

may affect the transport of chlorides. This is simply because the diffusion coefficient of chloride ions can be affected by the size of pores, and thus so does by the crack width if the crack is sufficiently small.

4.3.3. Volume fractions of damage zones

Figs. 23–25 show the comparison of concentration distribution profiles focusing on the effect of volume fraction of damage zones (the sizes of individual damage zones in the models are kept the same). In general, the obtained results in this set of numerical tests are extremely similar to what is showed in Figs. 20–22. If the damage length is fixed, the changing of volume fraction of damage zones does little impact on the chloride migration (Figs. 23 and 24). In addition, the more damage zones are contained, the more chlorides are transported (Fig. 25). Since the damage zones are all centrally located in one column in the simulated concrete, the increase of crack number is only along the y-axis which is perpendicular to the direction of electric field. Therefore, the effects resulted by damage width and volume fraction on the chloride migration are very close.

5. Summary

This study has presented a numerical investigation on the chloride migration in cracked concretes. By treating the concrete as a heterogonous and a homogenous material with taking into account the ionic interaction between different ionic species involved in the concrete pore solution, numerical simulations have been performed, from which the following conclusions can be drawn.

(1) Ionic interactions of multi-species are significant for studying the chloride migration in cracked concrete. The multi- and single-component models have totally distinct transport features, not only for the electrostatic potential distributions but also for the chloride penetration behaviours.
(2) The migration wave front in the cracked concrete travels at two distinct rates. One occurs in the uncracked part of concrete and its speed is similar to that performed in the normal concrete transport models; the other one occurs only in the damage zones and gets much larger speed than that in the non-damage bulk mortar, acting like shock waves, which take a shortcut through the damage zones.
(3) Under the action of an externally applied DC voltage, the damage length, which is exactly parallel to the electric field, dominates the migration rate in the present multi-component model, whereas the mesoscale damage width, the volume fraction of damage zones has little impact on the chloride migration, either in damage or non-damage areas. Additionally, according to the results of sensitivity analysis, the effects of different damage width and volume fraction on the chloride migration are very close.
(4) The analysis of concrete of multiple cracks suggests there is a "pollution" effect, which can disrupt the chloride migration. This 'pollution' effect is likely due to the local diffusion caused by dense array of multiple cracks.

Acknowledgments

The authors would like to thank the support from the European Research Council via a research grant (FP7-PEOPLE-2011-IRSES-294955). The second author would also like to thank the support from the (i) Project of National Natural Science Foundation of China (51378308); (ii) Specialized Research Fund for the Doctoral Program of Higher Education of China (20130073120074); and (iii) Innovation Program of Shanghai Municipal Education Commission (14ZZ027). The third author also appreciates the support from the Fundamental Research Funds for the Central Universities (2014FZA4020) and the Natural Science Foundation of China (51408537).

References

[1] S. Jacobsen, J. Marchand, L. Boisvert, Cem. Concr. Res. 26 (1996) 869–881.
[2] B. Gérard, J. Marchand, Cem. Concr. Res. 30 (2000) 37–43.
[3] J. Paulsson-Tralla, J. Silfwerbrand, ACI Mater. J. 99 (2002) 27–36.
[4] O. Garces Rodriguez, R.D. Hooton, ACI Mater. J. 100 (2003) 120–126.
[5] P.P. Win, M. Watanabe, A. Machida, Cem. Concr. Res. 34 (2004) 1073–1079.
[6] E. Kato, Y. Kato, T. Uomoto, J. Adv. Concr. Technol. 3 (2005) 85–94.
[7] M. Sahmaran, J. Mater. Sci. 42 (2007) 9131–9136.
[8] A. Djerbi, S. Bonnet, A. Khelidj, V. Baroghel-bouny, Cem. Concr. Res. 38 (2008) 877–883.
[9] M. Ismail, A. Toumi, R. Francois, Cem. Concr. Res. 38 (2008) 1106–1111.
[10] T. Ishida, P.O. Iqbal, H.T.L. Anh, Cem. Concr. Res. 39 (2009) 913–923.
[11] S.Y. Jang, B.S. Kim, B.H. Oh, Cem. Concr. Res. 41 (2011) 9–19.
[12] S.S. Park, S.J. Kwon, S.H. Jung, S.W. Lee, Constr. Build. Mater. 27 (2012) 597–604.
[13] C. Leung, D. Hou, J. Mater. Civ. Eng. (2014) 04014122, http://dxdoi.org/10.1061/(ASCE)MT.1943-5533.0001057.
[14] L. Marsavina, K. Audenaert, G. De Schutter, N. Faur, D. Marsavina, Constr. Build. Mater. 23 (2009) 264–274.
[15] L. Wang, T. Ueda, J. Adv. Concr. Technol. 9 (2011) 241–249.
[16] B. Šavija, J. Pacheco, E. Schlangen, Cement Concr. Compos. 42 (2013) 30–40.
[17] D.P. Bentz, E.J. Garboczi, Y. Lu, N. Martys, A.R. Sakulich, W.J. Weiss, Cement Concr. Compos. 38 (2013) 65–74.
[18] B. Šavija, M. Luković, E. Schlangen, Cem. Concr. Res. 61–62 (2014) 49–63.
[19] E. Schlangen, J.G.M. Van Mier, Mater. Struct. 25 (1992) 534–542.
[20] E. Schlangen, Z. Qian, J. Multiscale Model. 1 (2009) 245–261.
[21] J.E. Bolander, S. Berton, Cement Concr. Compos. 26 (2004) 861–871.
[22] P. Grassl, Cement Concr. Compos. 31 (2009) 454–460.
[23] S. Shahbeyk, M. Hosseini, M. Yaghoobi, Comput. Mater. Sci. 50 (2011) 1973–1990.
[24] F. Bernard, S. Kamali-Bernard, Comput. Mater. Sci. 61 (2012) 106–115.
[25] S. Dehghanpoor Abyaneh, H.S. Wong, N.R. Buenfeld, Comput. Mater. Sci. 78 (2013) 63–73.
[26] S. Dehghanpoor Abyaneh, H.S. Wong, N.R. Buenfeld, Comput. Mater. Sci. 87 (2014) 54–64.
[27] G.A. Narsillo, R. Li, P. Pivonka, D.W. Smith, Cem. Concr. Res. 37 (2007) 1152–1163.
[28] B. Johannesson, K. Yamada, L.O. Nilsson, Y. Hosokawa, Mater. Struct. 40 (2007) 651–665.
[29] E. Samson, J. Marchand, Comput. Struct. 85 (2007) 1740–1756.
[30] K. Krabbenhoft, J. Krabbenhoft, Cem. Concr. Res. 38 (2008) 77–88.
[31] J. Xia, L.Y. Li, Constr. Build. Mater. 39 (2013) 51–59.
[32] Q.F. Liu, L.Y. Li, D. Easterbrook, J. Yang, Eng. Struct. 42 (2012) 201–213.
[33] M.M. Jensen, B. Johannesson, M.R. Geiker, Comput. Mater. Sci. 92 (2014) 213–223.
[34] Q.F. Liu, D. Easterbrook, J. Yang, L.Y. Li, Eng. Struct. 86 (2015) 122–133.
[35] L.Y. Li, C.L. Page, Comput. Mater. Sci. 9 (1998) 303–308.
[36] F. Frizon, S. Lorente, J.P. Ollivier, P. Thouvenot, Comput. Mater. Sci. 27 (2003) 507–516.
[37] O. Truc, J.P. Ollivier, L.O. Nilsson, Cem. Concr. Res. 30 (2000) 1581–1592.
[38] Y. Wang, L.Y. Li, C.L. Page, Comput. Mater. Sci. 20 (2001) 196–212.
[39] A. Toumi, R. Francois, O. Alvarado, Cem. Concr. Res. 37 (2007) 54–62.
[40] Y. Liu, X. Shi, Constr. Build. Mater. 27 (2012) 450–460.
[41] Q.F. Liu, J. Xia, D. Easterbrook, J. Yang, L.Y. Li, Constr. Build. Mater. 70 (2014) 410–427.
[42] L. Tang, L.O. Nilsson, ACI Mater. J. 89 (1993) 49–53.
[43] NT-Build 492, Nordtest method: concrete, mortar and cement-based repair materials: chloride migration coefficient from non-steady-state migration experiments, 1999.
[44] AASHTO TP 64-03, Standard method of test for prediction of chloride penetration in hydraulic cement concrete by the rapid migration procedure, American Association of State Highway and Transportation Officials, Washington, 2003.
[45] D.R. Lankard, J.E. Slatter, W.A. Holden, D.E. Niest. Neutralization of chloride in concrete, FHWA Report No. FHWA-RD-76-6, Battelle Columbus Laboratories, 1975.
[46] Q.F. Liu. Multi-phase modelling of multi-species ionic migration in concrete. PhD Thesis, University of Plymouth, 2014.
[47] L. Tang, L.O. Nilsson, Cem. Concr. Res. 23 (1993) 247–253.
[48] T. de Larrard, B. Bary, E. Adamc, F. Kloss, Comput. Mater. Sci. 72 (2013) 1–14.
[49] L.Y. Li, J. Xia, Constr. Build. Mater. 26 (2012) 295–301.
[50] S. Diamond, J.D. Huang, Cement Concr. Compos. 23 (2001) 179–188.
[51] J.M. Gao, C.X. Qian, H.F. Liu, B. Wang, L. Li, Cem. Concr. Res. 35 (2005) 1299–1304.
[52] S. Caré, E. Hervé, Transport Porous Media 56 (2004) 119–135.
[53] J.J. Zheng, X.Z. Zhou, Mater. Struct. 40 (2007) 693–701.
[54] J.Y. Jiang, G.W. Sun, C.H. Wang, Constr. Build. Mater. 39 (2013) 134–138.
[55] L.Y. Li, C.L. Page, Corros. Sci. 42 (12) (2000) 2145–2165.
[56] A. Caporale, L. Feo, R. Luciano, Compos. Part B Eng. 65 (2014) 124–130.